

## OBSERVING QUARK-GLUON PLASMA WITH STRANGE HADRONS

JEAN LETESSIER

*Laboratoire de Physique Théorique et Hautes Energies\**  
*Université Paris 7, 2 place Jussieu, F-75251 Cedex 05*

and

JOHANN RAFELSKI†

*Department of Physics, University of Arizona, Tucson, AZ 85721*

We review the methods and results obtained in an analysis of the experimental heavy ion collision research program at nuclear beam energy of 160–200A GeV. We study strange, and more generally, hadronic particle production experimental data. We discuss present expectations concerning how these observables will perform at other collision energies. We also present the dynamical theory of strangeness production and apply it to show that it agrees with available experimental results. We describe strange hadron production from the baryon-poor quark-gluon phase formed at much higher reaction energies, where the abundance of strange baryons and antibaryons exceeds that of nonstrange baryons and antibaryons.<sup>a</sup>

---

<sup>a</sup>PACS: 12.38.Mh, 25.75.-q, 25.75.Dw, 25.75.Ld

### 1. Introduction and Overview

#### 1.1. Introduction

The study of highly excited and dense hadronic matter by means of ultra-relativistic nuclear collisions is a relatively novel area of research at the border between nuclear and particle physics. As such it, is in a rapid experimental and theoretical evolution. The primary goal of research in this field is the creation and investigation of elementary (particle) matter under extreme density and temperature conditions. The existence of a novel non-nuclear high temperature phase of elementary matter is an unavoidable consequence of the current knowledge about the strong nuclear interaction, rooted in the theory of strong interactions, the quantum field theory of quarks and gluons called quantum chromodynamics (QCD).<sup>1,2</sup>

Discovery and study of quark-gluon plasma (QGP), a ‘deconfined’ state consisting of mobile, color-charged quarks and gluons, is the objective of the relativistic heavy ion experimental research program underway at the Relativistic Heavy Ion Collider (RHIC) at Brookhaven National Laboratory (BNL), New York, and at the

---

\*LPTHE, Univ. Paris 6 et 7 is: Unité mixte de Recherche du CNRS, UMR7589.

†Supported by U.S. Department of Energy under grant DE-FG03-95ER40937.

Super Proton Synchrotron (SPS) accelerator at the European Organization for Nuclear Research (CERN), Geneva.<sup>3</sup> In a recent half day long workshop, and in an accompanying press release in February 2000 the CERN laboratory has formally announced that it views the collective evidence available today in their seven relativistic nuclear collision experiments as being conclusive: “. . . *A common assessment of the collected data leads us to conclude that we now have compelling evidence that a new state of matter has indeed been created, at energy densities which had never been reached over appreciable volumes in laboratory experiments before and which exceed by more than a factor 20 that of normal nuclear matter. The new state of matter found in heavy ion collisions at the SPS features many of the characteristics of the theoretically predicted quark-gluon plasma. . .*”<sup>4</sup>

This research program has been developed over the past two decades in order to study the properties of elementary matter at conditions similar to those seen in the very early universe  $30\mu\text{s}$  after the big-bang, before the temperature decreases to about  $T = 150\text{ MeV} \approx 1.7 \cdot 10^{12}\text{ K}$ . It has been many times argued that it is possible to achieve a laboratory recreation of this condition in a small-bang relativistic nuclear collision. The question is at what collision energy the transition to a color deconfined QGP phase first occurs. Early suggestion has been that this could occur at an intrinsic available energy per participating nucleon as low as 4 and 8 times the nucleon mass, corresponding to the range 30 and  $120A\text{ GeV}$  per nucleon beam energy in fixed target experiments.<sup>5</sup>

The conditions in the early universe and those created in nuclear collision experiments differ somewhat: whereas the primordial quark-gluon plasma survived for about  $30\mu\text{s}$  in the big bang, the comparable conditions in nuclear collisions are not expected to last for more than  $10^{-22}\text{ s}$  due to the rapid explosion of the hot matter “fireball”. Moreover, in the matter created in heavy ion collisions quarks are expected to outnumber antiquarks noticeably due to the baryon content of the colliding nuclei, whereas the net relative excess of the quarks over antiquarks in the universe was less than  $10^{-9}$ .

Numerical simulations of QCD suggest that the nature of the transformation between the hadronic and quark-gluon phases can change drastically as the values of the parameters of the theory are varied.<sup>6,7,8</sup> Recent analytical studies of the phase properties of QCD have supported the conclusion that the dependence on the net baryon density (baryochemical potential) is especially interesting.<sup>9,10</sup> Perhaps the most fundamentally important observable in this context is the latent heat associated with the breaking of color bonds among quarks, leading to the deconfinement of quarks. An experimental determination of this quantity and its dependence on beam energy would be of great scientific interest.

Strange particle signatures for the formation and evolution of the deconfined quark-gluon phase of elementary matter form a significant cornerstone of experimental QGP discovery. This subject has been developed quite intensely for the past 20 years.<sup>11,12,13,14,15,16</sup> The enabling difference in physics between confined and deconfined matter concerning strange particle signatures is rather simple:

- In the QGP phase the particle density is high enough and the strange flavor production energy threshold low enough to assure that a high abundance of strangeness can actually be produced on the time scale available<sup>12,13,16,17,18</sup> while in the confined matter phase this has been shown not to be the case,<sup>13,19</sup> as long as one wants to remain consistent with other experimental results.
- Population at, and even in excess, of chemical equilibrium of hadron phase space occupancies occurs only when the entropy rich QGP phase disintegrates rapidly and explosively into hadrons.<sup>13,15,16,20</sup>

There are several important and when viewed together, uniquely QGP characteristic predictions regarding strangeness, expected to occur should deconfinement set in. Specifically, the three pillars on which the QGP hypothesis stands when seen by means of strangeness flavor observables are:

- 1) matter-antimatter symmetry as seen for directly emitted strange baryon and antibaryon particles in the  $m_{\perp}$ -spectral shape and strange quark fugacity;
- 2) (multi)strange baryon and antibaryon enhancement increasing with strangeness content;
- 3) enhancement of the (specific) strangeness flavor yield per reaction participant (baryon), by a factor 1.5–3 at SPS conditions, the value depending on what is used as baseline, and if one looks alone at the central rapidity region, where this effect is strongest, or considers the global strangeness yield, including the kinematic domains of projectile and target fragmentation.

*All three predictions have recently been confirmed at the current SPS energy range 158 GeV per nucleon for Lead (Pb), and some also for 200 GeV per nucleon Sulphur (S) induced reactions.*

Examples and stepping stones are in particular:

- 1) The WA97 collaboration reported a detailed study of transverse mass strange baryon and antibaryon spectra which show a highly unusual symmetry between strange baryon and antibaryon sector.<sup>21</sup>
- 2) A detailed analysis of Pb–Pb results by the WA97 collaboration has demonstrated, comparing p–p, p–A with A–A results, a strong enhancement in the pertinent (multi) strange baryon and antibaryon yields, increasing with strangeness content.<sup>22,23,24,25</sup> The results of the NA49 collaboration are consistent with these findings.<sup>26</sup> The WA85 collaboration also finds an enhancement of multi-strange baryons and antibaryons, increasing with strangeness content in S-induced reactions.<sup>27</sup>
- 3a) Strangeness enhancement at mid-rapidity has been observed in S-induced reactions by the experiments NA35,<sup>28</sup> WA85 and WA94,<sup>29</sup> and NA44.<sup>30</sup> In the larger Pb–Pb reaction system strangeness enhancements are reported by WA97,<sup>22,23,31</sup> NA49,<sup>32</sup> and NA44.<sup>33</sup> Results of the experiment NA52 suggest further that the onset of strangeness enhancement occurs rather suddenly as the centrality of the collisions and thus the size of participating matter rises above baryon number  $B = 40$ –50.<sup>34</sup>

- 3b) Global Strangeness enhancement has been observed both in S-induced and

in Pb-Pb reactions by the NA35,<sup>28</sup> and NA49,<sup>32</sup> experiments.

In this article, we also rely in many aspects of this discussion indirectly on other experimental results of NA35 and NA49 collaborations, which offer a global view on particle production pattern considering the large kinematic acceptance.<sup>35,36</sup> We will not discuss or use here other experimental discoveries which have contributed to the CERN announcement, which are not related to strangeness, such as  $J/\Psi$  suppression, dilepton and direct photon production. Readers interested in these topics should consult the list of experimental results.<sup>4</sup>

In view of many often intricate but, when analyzed, convincing experimental findings about strange particle production, the purpose of this article is to present a comprehensive and selfconsistent view on the understanding of the evidence comprised in strange hadron production for the formation of quark-gluon plasma at CERN, and to discuss resulting expectations how this observable will perform at RHIC. We address in this review:

- i) in section **2** the status of a analysis of the experimental data obtained at SPS,<sup>37</sup>
- ii) in section **3** the implications of these results for the understanding of the dense phase formed in these reactions,
- iii) in section **4** an adaptation of the dynamical theory of strangeness production in QGP to RHIC conditions,
- iv) in section **5** an application of these results to obtain predictions for hyperon yields from QGP at RHIC,
- v) in section **6** highlights of the results presented here and we draw our conclusions.

## 1.2. Overview

We introduce in section **2**, the Fermi-2000 model,<sup>16,44</sup> a straightforward elaboration of the original Fermi proposal,<sup>38</sup> that final state strongly interacting particles are produced with a probability commensurate to the size of the accessible phase space. In this approach, the hadron phase space is characterized to the required degree of accuracy by six parameters which have a clear physical meaning and can be in computed, and/or rather easily understood qualitatively, when their values have been determined by an analysis of the experimental data. The physical picture underlying the use of the statistical Fermi model in the 21st century is the sudden, explosive disintegration of a high temperature hadronic matter fireball, apparently consisting of deconfined quark-gluon matter. Since its proposal 50 years ago, the Fermi model has been subject to considerable scrutiny and adaptation, with Hagedorn's 'boiling' hadronic matter being the most important stepping stone.<sup>39</sup> The following were the relevant recent steps in the development of the statistical particle production description required to analyze the strange particle experimental results:

1. Considering the interest and considerable theoretical effort vested in understanding strange quark production mechanisms and the study of chemical equilibration processes,<sup>12,13</sup> it was a natural refinement to introduce an expression of chemical non-equilibrium in the number of strange quark pairs,

$\gamma_s \neq 1$ ,<sup>15</sup> into the analysis of strange hadrons.

2. In the analysis of the entropy content in S–W/Pb interactions,<sup>40</sup> we found entropy excess related to excess of meson abundance. This prompted us to explore possible nonequilibrium yield of mesons compared to that of baryons.<sup>41</sup>
3. Since the dense hadron fireball is subject to explosive disintegration, final state hadrons emerge from rapidly outward moving volume cells. In order to describe quantitatively spectra of hadronic particles, and their yields in restricted domains of phase space, such ‘collective’ matter flow motion needs to be modeled.<sup>41,42,43</sup>
4. Chemical (particle abundance changing) processes occurring at the time of hadronization do not generally lead to an equilibrium chemical yield of light quarks, and the chemical non-equilibrium is more pronounced if hadronization is a sudden process on the time scale of chemical quark equilibration. While this effect has been well accepted for strange quarks, as these need to be produced in microscopic processes, the need to introduce the light quark pair abundance parameter,  $\gamma_q \neq 1$ , was recognized rather late,<sup>44,45</sup> and is not yet widely accepted.

A data analysis we perform, allowing for all these effects, does not simply yield a set of ‘best’ parameters; rather:

- i) it offers a complete characterization of the phase space of hadrons and its occupancy, allowing one to extrapolate reliably the particle yields into kinematic domains not accessible at present;
- ii) it allows one to study and understand the magnitude of model parameters, so that we can safely to extrapolate their values to other reaction conditions, *e.g.*, from SPS to RHIC as will be done here;
- iii) it allows one to evaluate the physical properties of the phase space characterized by these parameters, which provides very precise information about the physical properties of the particle source. This in turn leads to the understanding of the nature of the dense fireball created in the heavy ion collision.

In order to pursue these aims, we need to reach considerable precision in the description of experimental results.

Our approach and objectives elaborate significantly on the now commonly accepted observation that all hadronic particles produced in strong interaction processes *qualitatively* satisfy statistical model predictions, as discovered and discussed in great detail by Rolf Hagedorn more than 30 years ago.<sup>39</sup> The fact that the statistical model indeed ‘works’ does not cease to amaze and impress.<sup>46,47</sup> At times this even provokes the hypothesis that ‘thermal’ abundances of hadrons could arise in some mysterious and unknown way,<sup>48</sup> and thus one could proceed to predict ‘thermal’ yields of hadrons, apparently believing that the statistical ‘thermal’ model substitutes for conventional particle production mechanisms. The recent proposal

by Bialas to consider the fluctuation of string tension is indeed suggesting how such an explanation could arise in p–p reactions.<sup>49</sup>

However, for reactions of large nuclei, the statistical description implies and exploits the result of repeated occurrence of microscopic collision reactions, and the associated approach to an equilibrium distribution shape, and *independently*, also approach to chemical particle abundance equilibrium. This is independent of the above described possibility that in elementary reaction systems equilibration is possibly a consequence of microscopic properties of strong interactions. Our discussion of A–A reactions thus aims at an improvement of the statistical description beyond the ‘thermal’ model, such that we can deal with standard deviation errors comparing theory and experiment, as is common in the field of particle and nuclear physics.

The way we set up the Fermi-2000 model represents the microscopic processes that are occurring, and of course there are limits to this description. For example, primary high energy initial interactions can produce heavy quark flavor which could not arise from the generally softer interactions occurring in the kinetically equilibrated system (an example is expected production of charm at RHIC<sup>50,51</sup>). More generally, an acceptable failure of a statistical description is the one which under-predicts the yield of rarely produced particles. For this reason, it is necessary to scrutinize the validity of the statistical description, at least for the most rarely produced hadrons.

Pertinent results of a complete analysis of the Pb–Pb system are presented in section 3. We describe abundances and spectra of hadronic particles observed by both the wide acceptance NA49-experiment and the central rapidity (multi)strange (anti)baryon WA97-experiment. Our method of analysis shows that both these families of results obtained with widely different methods are consistent and it allows us to reach the required precision in their description. This objective could be reached only after we have introduced light quark chemical non-equilibrium and allowed that the all strange  $\Omega(sss)$  and  $\bar{\Omega}(\bar{s}\bar{s}\bar{s})$  hadrons are enhanced beyond their statistical phase space yield, a point we will discuss in greater detail in subsection 3.4 below. These developments occurred after the last comprehensive review of the subject appeared,<sup>52</sup> and after the extensive SPS-Pb-beam experimental results became available. The introduction of light quark chemical nonequilibrium has had a significant impact on the determination of the physical properties of the hadron emitting source, as it allows for a considerable reduction of the chemical freeze-out temperature: specifically we have determined that  $T_f = 143 \pm 5$  MeV, we have also included here an estimate of the systematic error, for the temperature at which practically all strange hadrons are formed. This result is nearly 30 MeV below values that one might infer otherwise in a qualitative study of the statistical hadron yields.<sup>46,47,53</sup>

This relatively low freeze-out temperature is consistent with the result that the chemical freeze-out parameters determine correctly the shape of hadron  $m_{\perp}$ -spectra, which suggests that after the deconfined QGP source has dissociated the resulting

hadrons are practically free-streaming and thus that thermal and chemical freeze-out do not differ much if at all. This particle production scheme is called *sudden hadronization*.<sup>13,15</sup> In terms of a microscopic model it occurs when hadronic particles are produced either in:

- a) an evaporation process from a hot expanding surface, or
- b) a sudden global hadronization process of exploding, possibly super-cooled deconfined matter.

Experimental evidence supporting the picture of sudden QGP hadronization is most directly derived from the baryon-antibaryon transverse mass  $m_{\perp}$ -spectral symmetry. Another piece of evidence for a sudden hadronization is the chemical overabundance of light quark pairs in hadronization and the associated maximization of entropy density in hadron phase space as will be discussed in subsection **2.3**. Not to be forgotten is the original observation about experimental data that has led to the data interpretation in terms of the sudden hadronization model<sup>15</sup>: the strange quark fugacity as measured by emitted strange hadrons implies a source with freely moving strange  $s$  and antistrange  $\bar{s}$  quarks such that  $\langle s - \bar{s} \rangle = 0$ , a point we will discuss in subsection **2.2**.

In subsection **3.3**, we study in depth the phenomenon of strangeness enhancement and show that the rather precise analysis results we obtain are in excellent agreement with the theoretically computed strangeness yields, assuming formation of the QGP phase. We also show that, in the case of Pb–Pb, the explosive disintegration of the dense QGP fireball leads to an overpopulation of the strangeness phase space abundance, and show that theoretical results are again in good agreement with the results of the data analysis. The initial temperatures for this agreement to occur are in the range  $260 < T_{\text{ch}} < 320$ , which values we obtain from models of collision dynamics.

In section **4**, we develop the theoretical method which leads to the finding of overpopulated strangeness phase space discussed in subsection **3.3**. This, at a first sight surprising result, occurs due to early freeze-out of strangeness abundance in a rapid explosive evolution of the QGP fireball. We find a similar non-equilibrium result, in section **5**, for RHIC condition in presence of transverse expansion which increases the speed at which QGP dilutes. We explore the dynamics of the phase space occupancy, rather than particle density, which allows us to eliminate much of the dependence on the dynamical flow effects by incorporating in the dynamics considered the hypothesis of entropy conserving matter flow and evolution.

Exploiting the experience with SPS data analysis, we are able to consider, in section **5**, strange particle production at RHIC. We obtain an unexpected particle abundance pattern: during the hadronization of the baryon-poor RHIC-QGP phase there is considerable advantage for strangeness flavor to stick to baryons and antibaryons. This can be easily understood realizing that production of strange (anti)baryons is favored over production of kaons by the energy balance, *i.e.*:  $E(\Lambda + \pi) < E(N+K)$ . Moreover, at RHIC there are a high number of strange quarks per baryon available, and in this strangeness bath just a few (anti)baryons will manage

to emerge without strangeness content. We thus expect and find in detailed study in section 5 that hyperon production dominates baryon production, *i.e.*, most baryons and antibaryons produced will be strange. We consider this result to be a unique consequence of the sudden QGP hadronization scenario observed at SPS and hope and expect that hyperon dominance should, when observed at RHIC, be generally accepted as proof of formation of the deconfined phase of nuclear matter. This phenomenon shows how much more pronounced will be the physics of strangeness in QGP at RHIC, as compared to the ten times lower SPS energy range.

## 2. Contemporary Fermi Model of Hadron Production

### 2.1. Phase space and parameters

The relative number of final state hadronic particles freezing out from, *e.g.*, a thermal quark-gluon source is obtained noting that the fugacity  $f_i$  of the  $i$ -th emitted composite hadronic particle containing  $k$ -components is derived from fugacities  $\lambda_k$  and phase space occupancies  $\gamma_k$ :

$$N_i \propto e^{-E_i/T_f} f_i = e^{-E_i/T_f} \prod_{k \in i} \gamma_k \lambda_k. \quad (1)$$

We study chemical properties of light quarks  $u, d$  jointly, denoting these by a single index  $q$  and also consider chemical properties of strange quarks  $s$ . Thus as seen in Eq. (1), we study particle production in terms of five statistical parameters. In addition there is at least one matter flow velocity parameter. The six parameters which characterize the accessible phase space of hadronic particles made of light quarks ‘q’ and strange quarks ‘s’ and their natural values, assuming a QGP source, are in turn:

1)  $\lambda_s$ : The value of strange quark fugacity  $\lambda_s$  can be obtained from the requirement that strangeness balances,  $\langle N_s - N_{\bar{s}} \rangle = 0$ , which for a source in which all  $s, \bar{s}$  quarks are unbound and thus have symmetric phase space, implies  $\lambda_s = 1$ . However, the Coulomb distortion of the strange quark phase space plays an important role in the understanding of this constraint for Pb–Pb collisions,<sup>54</sup> leading to the Coulomb-deformed value  $\lambda_s \simeq 1.1$ , as discussed in next subsection.

2)  $\gamma_s$ : The strange quark phase space occupancy  $\gamma_s$  can be computed, and will be studied in this review in detail within the framework of kinetic theory.<sup>12,16</sup> For a rapidly expanding system the production processes will lead to an over-saturated phase space with  $\gamma_s > 1$ . The difference between the two different types of chemical parameters  $\lambda_i$  and  $\gamma_i$  is that the phase space occupancy factor  $\gamma_i$  regulates the number of pairs of flavor ‘ $i$ ’, and hence applies in the same manner to particles and antiparticles, while fugacity  $\lambda_i$  applies only to particles, while  $\lambda_i^{-1}$  is the antiparticle fugacity.

3)  $\lambda_q$ : The light quark fugacity  $\lambda_q$ , or equivalently, the baryochemical potential:

$$\mu_B = 3T_f \ln \lambda_q, \quad (2)$$



regulate the baryon density of the fireball and hadron freeze out. This density can vary dependent on the energy and size of colliding nuclei, and thus the value of  $\lambda_q$  is not easily predicted. However, since we know the energy per baryon content in the incoming nuclei, if we assume that the deposition of the baryon number and energy ('stopping') is similar, we know the energy per baryon content in the fireball.<sup>16</sup> This qualitative knowledge can be used in a study of equations of state applicable to the dense fireball to establish a constraint.

4)  $\gamma_q$ : The equilibrium phase space occupancy of light quarks  $\gamma_q$  is expected to significantly exceed unity to accommodate the excess entropy content in the plasma phase.<sup>40,41</sup> There is an upper limit:

$$\gamma_q < \gamma_q^c \equiv e^{m_\pi/2T}, \quad (3)$$

which arises if all pions produced are simultaneously present, forming a Bose gas. We will address this effect in subsection **2.3**.

5)  $T_f$ : The freeze-out temperature  $T_f$  is expected to be not much different from the Hagedorn temperature  $T_H \simeq 160$  MeV,<sup>39</sup> which characterized particle production in proton-proton reactions.

6)  $v_c$ : The collective expansion velocity  $v_c$  is expected to remain below the relativistic sound velocity<sup>16</sup>:

$$v_c \leq 1/\sqrt{3}. \quad (4)$$

When the source emitting the free streaming particles is undergoing local collective flow motion, spectra of particles emitted are described by replacing the Boltzmann factor in Eq. (1) by:

$$\begin{aligned} e^{-E_i/T} &\rightarrow \frac{1}{2\pi} \int d\Omega_v \gamma_c (1 - \vec{v}_c \cdot \vec{p}_i/E_i) e^{-\frac{\gamma_c E_i}{T} (1 - \vec{v}_c \cdot \vec{p}_i/E_i)}, \\ \gamma_c &= \frac{1}{\sqrt{1 - \vec{v}_c^2}}, \end{aligned} \quad (5)$$

a result which can be intuitively obtained by a Lorentz transformation between an observer on the surface of the fireball, and one at rest in the laboratory frame. Formal derivation of this and more elaborated results requires a considerably more precise framework.<sup>42</sup>

The resulting yields of final state hadronic particles are most conveniently characterized taking the Laplace transform of the accessible phase space. This approach generates a function which in its mathematical properties is identical to the partition function. For example for the open strangeness sector we find, for the case  $v_c = 0$ :

$$\begin{aligned} \ln \mathcal{Z}_s = \frac{VT^3}{2\pi^2} &\{ (\lambda_s \lambda_q^{-1} + \lambda_s^{-1} \lambda_q) \gamma_s \gamma_q F_K + (\lambda_s \lambda_q^2 + \lambda_s^{-1} \lambda_q^{-2}) \gamma_s \gamma_q^2 F_Y \\ &+ (\lambda_s^2 \lambda_q + \lambda_s^{-2} \lambda_q^{-1}) \gamma_s^2 \gamma_q F_\Xi + (\lambda_s^3 + \lambda_s^{-3}) \gamma_s^3 F_\Omega \}. \end{aligned} \quad (6)$$

The integrated momentum phase space factors  $F_i$  for kaons  $i = K$ , single strange hyperons  $i = Y$ , doubly strange cascades  $i = \Xi$  and triply strange omegas  $i = \Omega$

are:

$$F_i = \sum_j g_{i_j} W(m_{i_j}/T), \quad W(x) = x^2 K_2(x). \quad (7)$$

$g_{i_j}$  is the statistical degeneracy of each contributing hadron resonance ‘ $j$ ’ of the kind ‘ $i$ ’ in the  $\sum_j$ , which comprise all known strange hadron resonances.  $K_2$  is the modified Bessel function which arises from the relativistic phase space integral of the thermal particle distribution  $f(\vec{p}) \propto e^{-\sqrt{m^2+p^2}/T}$ . It is important to keep in mind that:

- a) Eq. (6) does not require formation of a phase comprising a gas of hadrons, but is not inconsistent with such a step in evolution of the fireball; in that sense it is not a partition function, but just a look-alike object arising from the Laplace transform of the accessible phase space, and
- b) the final particle abundances measured in an experiment are obtained after all unstable hadronic resonances ‘ $j$ ’ are allowed to disintegrate, contributing to the yields of stable hadrons;
- c) the unnormalized particle multiplicities arising are obtained differentiating Eq. (6) with respect to particle fugacity. The relative particle yields are simply given by ratios of corresponding chemical factors, weighted with the size of the momentum phase space accepted by the experiment. For particles showing the same spectral shape comparison of normalization of  $m_\perp$  spectra suffices, *e.g.*, Ref. <sup>15</sup>:

$$\frac{\Xi^-(dss) \Big|}{\Lambda(dss) \Big|_{m_\perp}} = \frac{g_\Xi \gamma_d \gamma_s^2 \lambda_d \lambda_s^2}{g_\Lambda \gamma_d^2 \gamma_s \lambda_d^2 \lambda_s}. \quad (8)$$

$g_i$  are the spin statistical factors of the states considered. Similarly:

$$\frac{\overline{\Xi^-(dss)} \Big|}{\overline{\Lambda(dss)} \Big|_{m_\perp}} = \frac{g_\Xi \gamma_d \gamma_s^2 \lambda_d^{-1} \lambda_s^{-2}}{g_\Lambda \gamma_d^2 \gamma_s \lambda_d^{-2} \lambda_s^{-1}}. \quad (9)$$

When acceptance is limited to central rapidity, and significant flow is present considerable effort must be made to introduce appropriate phase space weights.

- d) In some experimental data it is important to distinguish the two light quark flavors as is in fact the case in the two above examples. This can be incorporated considering how the average light quark fugacity varies between both light quark species,<sup>15</sup> and assuming that the phase space occupancies are equal.

We consider, for SPS energy range, the radial flow model, which is without doubt the simplest of the reasonable and expected matter flow cases possible, in view of the behavior of global observables seen in these experiments. As the results below show, this suffices to assess the impact of collective flow on the data analysis originally developed to be as little as possible sensitive to collective matter flow, even when particle yields in highly restricted regions of  $m_\perp$ ,  $y$  are considered. The collective source flow can completely change the shape of momentum distribution of particle produced, though of course it leaves unchanged the total particle yield, which is the integral sum of particle multiplicity over the entire phase space of the flow

spectrum. However, particles of different mass experience differing flow effects when  $m_{\perp}$ ,  $y$  acceptance cuts are present. Moreover, particles can freeze-out at slightly different conditions. In order to limit the influence of the practically unknown collective flow structure on particle yields in limited domains of the accessible phase space, we study compatible particle ratios: these are yield ratios obtained in a restricted domain of  $m_{\perp}$ ,  $y$ , for particles of similar mass and believed to have a similar interaction strength with the matter background.

We now will address in turn two special topics, which slightly contradict expectations, and thus require more attention. Firstly, we review the the properties of the strange quark fugacity  $\lambda_s$ , which is sensitive to the possible asymmetry between strange and antistrange quarks in the source. The importance of this parameter is that it potentially helps distinguish the confined from deconfined phase: while in the baryon-rich confined phase the requirement of strangeness conservation implies that  $\lambda_s > 1$ , in the deconfined phase the symmetry between phase space of strange and antistrange quarks implies  $\lambda_s \simeq 1$ . Following this, we address in more detail case of pions,<sup>56</sup> which is exceptional since we will be considering rather large values of  $\gamma_q > 1.5$ . As we shall see, the pion gas emerging from the QGP phase is strongly influenced by Bose correlation effects; in fact it is close to satisfying the Bose condensation condition.

## 2.2. Coulomb force

It has been recognized for a long time that the Coulomb force can be of considerable importance in the study of relativistic heavy ion collisions. It plays an important role in the HBT analysis of the structure of the particle source.<sup>57</sup> We show that the analysis of chemical properties at freeze-out is also subject to this perturbing force, and in consideration of the precision reached in the study of particle ratios, one has to keep this effect in mind.

We consider a Fermi gas of strange and antistrange quarks, allowing that the Coulomb potential  $V$  established by the excess charge of the colliding nuclei distorts significantly the phase space. Within a relativistic Thomas-Fermi phase space occupancy model,<sup>58</sup> and allowing for finite temperature in QGP we have<sup>54</sup>:

$$\langle N_s - N_{\bar{s}} \rangle = \int_{R_f} g_s \frac{d^3r d^3p}{(2\pi)^3} \left[ \frac{1}{1 + \gamma_s^{-1} \lambda_s^{-1} e^{(E(p) - \frac{1}{3}V(r))/T}} - \frac{1}{1 + \gamma_s^{-1} \lambda_s e^{(E(p) + \frac{1}{3}V(r))/T}} \right], \quad (10)$$

which clearly cannot vanish for  $V \neq 0$  in the limit  $\lambda_s \rightarrow 1$ . In Eq. (10) the subscript  $R_f$  on the spatial integral reminds us that only the classically allowed region within the fireball is covered in the integration over the level density;  $E = \sqrt{m^2 + \vec{p}^2}$ , and for a uniform charge distribution within a radius  $R_f$  of charge  $Z_f$ :

$$V = \begin{cases} -\frac{3}{2} \frac{Z_f e^2}{R_f} \left[ 1 - \frac{1}{3} \left( \frac{r}{R_f} \right)^2 \right], & \text{for } r < R_f; \\ -\frac{Z_f e^2}{r}, & \text{for } r > R_f. \end{cases} \quad (11)$$

One obtains a rather precise result for the range of parameters of interest to us using the Boltzmann approximation:

$$\langle N_s - N_{\bar{s}} \rangle = \gamma_s \left\{ \int g_s \frac{d^3 p}{(2\pi)^3} e^{-E/T} \right\} \int_{R_f} d^3 r \left[ \lambda_s e^{\frac{V}{3T}} - \lambda_s^{-1} e^{-\frac{V}{3T}} \right]. \quad (12)$$

The Boltzmann limit allows us also to verify and confirm the signs: the Coulomb potential is negative for the negatively charged  $s$ -quarks with the magnitude of the charge,  $1/3$ , made explicit in the potential terms in all expressions above. We thus have<sup>54</sup>:

$$\tilde{\lambda}_s \equiv \lambda_s \lambda_Q^{1/3} = 1, \quad \lambda_Q \equiv \frac{\int_{R_f} d^3 r e^{\frac{V}{3T}}}{\int_{R_f} d^3 r}. \quad (13)$$

$\lambda_Q < 1$  expresses the Coulomb deformation of strange quark phase space.  $\lambda_Q$  is not a fugacity that can be adjusted to satisfy a chemical condition, since consideration of  $\lambda_i$ ,  $i = u, d, s$ , exhausts all available chemical balance conditions for the abundances of hadronic particles. The subscript  $R_f$ , in Eq. (13), reminds us that the classically allowed region within the dense matter fireball is included in the integration over the level density. Choosing  $R_f = 8$  fm,  $T = 140$  MeV,  $m_s = 200$  MeV, noting that the value of  $\gamma_s$  is practically irrelevant as this factor cancels in Boltzmann approximation, see Eq. (12), we find for  $Z_f = 150$  that the value  $\lambda_s = 1.10$  corresponds to  $R_f = 7.9$  fm. The Coulomb effect is thus relevant in central Pb–Pb interactions, while for S–Au/W/Pb reactions, similar analysis leads to a value  $\lambda_s = 1.01$ , little different from the value  $\lambda_s = 1$  expected in the absence of the Coulomb phase space deformation. Another way to understand the varying importance of the Coulomb effect is to note that while the Coulomb potential acquires in the Pb–Pb case a magnitude comparable to the quark chemical potential, it remains small on this scale for S–Au/W/Pb reactions.

### 2.3. Super-dense pion gas and chemical non-equilibrium

For pions composed of a light quark-antiquark pair, the chemical fugacity is  $\gamma_q^2$ , see Eq. (1). Thus the pion momentum space distribution has the Bose shape:

$$f_\pi(E) = \frac{1}{\gamma_q^{-2} e^{E_\pi/T} - 1}, \quad E_\pi = \sqrt{m_\pi^2 + p^2}. \quad (14)$$

The range of values for  $\gamma_q$  is bounded from above by the Bose singularity. When  $\gamma_q \rightarrow \gamma_q^c$ , Eq. (3), the lowest energy state (in the continuum limit with  $p \rightarrow 0$ ) will acquire macroscopic occupation and a pion condensate is formed. Formation of such a condensate ‘consumes’ energy without consuming entropy of the primordial high entropy QGP phase. On the other hand, as we shall see presently, when  $\gamma_q \rightarrow \gamma_q^c$  the entropy content of the pion gas initially grows! Thus while the development, directly from the QGP phase, of a pion condensate is not likely, the sudden hadronization of entropy rich QGP should lead to the limiting value  $\gamma_q \rightarrow \gamma_q^c$ , in order to more efficiently connect the entropy rich deconfined and the confined phases.

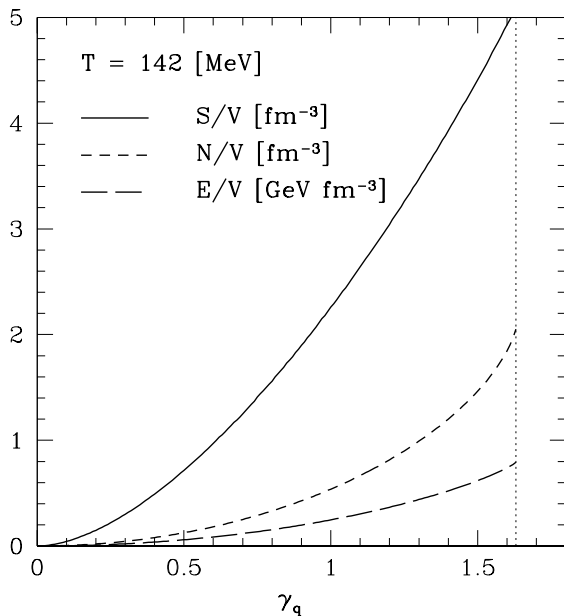


Fig. 1. Dependence of pion gas properties  $N/V$ -particle,  $E/V$ -energy and  $S/V$ -entropy density, as function of  $\gamma_q$  at  $T = 142$  MeV.

An interesting feature of such a mechanism of phase transition is that the chemical non-equilibrium reduces and potentially eliminates any discontinuity in the phase transition, which thus, in the experiment, will appear more like a phase transformation without critical fluctuations, even if theory implies a 1st order phase transition for statistical equilibrium system.

In Fig. 1, we show the physical properties of a pion gas as function of  $\gamma_q$  for a gas temperature  $T = 142$  MeV.<sup>56</sup> We see (solid line) that a large range of entropy density can be accommodated by varying the parameter  $\gamma_q$ . It is important to remember that in the hadronization of a quark-gluon phase it is relatively easy to accommodate energy density, simply by producing a few heavy hadrons. However, such particles being in fact non-relativistic at the temperature considered, are not effective carriers of pressure and entropy. However, as we see now in Fig. 1, the super-dense pion gas is just the missing element to allow a rapid hadronization process, since the entropy density is nearly twice as high at  $\gamma_q \simeq \gamma_q^c$  than at  $\gamma_q = 1$ . Without this phenomenon one has to introduce a mechanism that allows the parameter  $VT^3$  to grow, thus expanding either the volume  $V$  due to formation of so called mixed phase or invoking rise of  $T$  in so called reheating.

The specific properties of the super-dense pion gas are shown Fig. 2. In Fig. 2a, we relate the properties to the chemical equilibrium value  $\gamma_q = 1$  and we also show that the Boltzmann approximation is not qualitatively wrong, as long as  $\gamma_q < \gamma_q^c$ . In Fig. 2b, we see the relative change in energy per pion, (inverse of) entropy per pion, and energy per entropy. Interestingly, we note that the entropy per pion drops

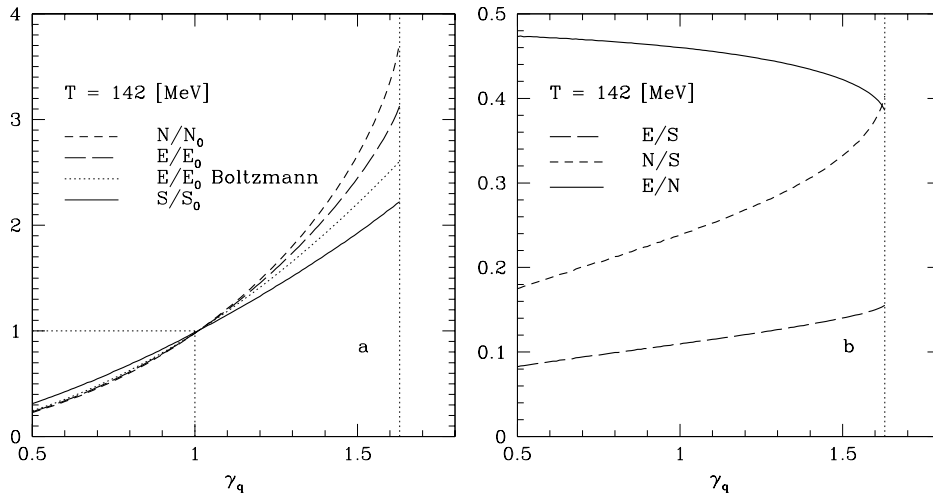


Fig. 2. Dependence of pion gas properties ( $N$ -particle,  $E$ -energy and  $S$ -entropy) density as function of  $\gamma_q$  for  $T = 142$  MeV. **a)** ratios relative to equilibrium value  $\gamma_q = 1$ ; **b)** relative ratios, thus  $E/N$ ,  $N/S$  and  $E/S$ .

as  $\gamma_q$  increases, and at the condensation point  $\gamma_q = \gamma_q^c$ , we can add pions without increase in entropy. We further note that a hadronizing gas will consume, at higher  $\gamma_q$ , less energy per particle, and that the energy per entropy is nearly constant.

It is important to remember that if the hadronization process were adiabatic, allowing a full equilibrium relaxation, naturally  $\gamma_i \rightarrow 1$  would arise: as is implicitly well known the value  $\gamma_i \rightarrow 1$  maximizes the entropy for a particle gas at fixed total energy, corresponding to the chemical equilibrium.<sup>59</sup> This result is easily found considering Boltzmann pion gas, and recalling in some detail the definition of entropy, since the standard equilibrium expressions do not apply:

$$S_{B,F} = \int \frac{d^3p d^3x}{(2\pi\hbar)^3} [\pm(1 \pm f(x,p)) \ln(1 \pm f(x,p)) - f(x,p) \ln f(x,p)], \quad (15)$$

$$\rightarrow V \int \frac{d^3p}{(2\pi\hbar)^3} f(p) \ln[e/f(p)], \quad (16)$$

where aside of ‘B,F’ (Bose, Fermi) also the Boltzmann limit for a homogeneous spatial distribution is shown explicitly.

Evaluating in Boltzmann limit the particle number and energy, we find that the factor  $\gamma_q^2$  becomes a normalization factor which describes the average occupancy of the phase space relative to the equilibrium value, and for entropy, we also find a logarithmic term:

$$N = \gamma_q^2 N|_{\text{eq}} \rightarrow aV\gamma_q^2 T^3, \quad (17)$$

$$E = \gamma_q^2 E|_{\text{eq}} \rightarrow 3aV\gamma_q^2 T^4, \quad (18)$$

$$S = \gamma_q^2 S|_{\text{eq}} + \ln(\gamma_q^{-2}) \gamma_q^2 N|_{\text{eq}} \rightarrow 4aV\gamma_q^2 T^3 + \ln(\gamma_q^{-2}) aV\gamma_q^2 T^3. \quad (19)$$

For massless pions,  $a = g/\pi^2$ , with pion degeneracy  $g = 3$ . Setting  $E = \text{Const.}$ , we eliminate  $T$  and find that the entropy as function of  $\gamma_q$  varies according to:

$$S|_{E=\text{Const.}} \propto \gamma_q^{\frac{1}{2}} (4 - \ln \gamma_q^2), \quad (20)$$

which has a very weak maximum at  $\gamma_q = 1$ ; note that at  $\gamma = 1.4$ , the entropy is at 98.3% of the value at  $\gamma = 1$ . At this point it is important to realize that the chemical equilibrium is much better defined for the more familiar case of a fixed temperature bath (and not an isolated fixed energy fireball discussed above): consider the free energy  $\mathcal{F}$  of the (non-interacting) relativistic gas at fixed temperature  $T$ . Since  $\mathcal{F} = E - TS$ , we combine Eqs. (17–19) and obtain in the Boltzmann limit,

$$\mathcal{F}^l = -aVT^4 \gamma_q^2 [1 + \ln(\gamma_q^{-2})], \quad (21)$$

which has a minimum for chemical equilibrium value  $\gamma_q = 1$ . However, one now finds that a change by factor 1.4 in  $\gamma_q$ , at fixed  $T$  leads to a change by 35% in the value of the free energy and even a greater change in entropy.

We conclude that, in adiabatic condition, the fireball would evolve to the maximum entropy equilibrium case  $\gamma_i = 1, i = q, s$ , the gain in entropy for an isolated system is in this limit very minimal. Thus for a system with rapidly evolving volume, we will in general find more effective paths to increase entropy, other than the establishment of the absolute chemical equilibrium. Hence the values we report  $\gamma_i \neq 1, i = q, s$ , are consistent with the present day understanding of explosive evolution of the hadronic matter fireball.

In a systematic study of the relevance of different physical parameters, the chemical non-equilibrium at hadron freeze-out has been shown to be a required ingredient in order to arrive at a precise interpretation of the experimental results on particle ratios  $R^j$  obtained at CERN. This is best seen considering the results for the statistical parameters obtained for the S–Au/W/Pb collisions,<sup>44</sup> and the associated total statistical error,

$$\chi_{\text{T}}^2 \equiv \frac{\sum_j (R_{\text{th}}^j - R_{\text{exp}}^j)^2}{(\Delta R_{\text{exp}}^j)^2}, \quad (22)$$

which are presented in table 1. We clearly see the gain in physical significance that is accomplished as chemical non-equilibrium is allowed for by releasing the fixed value  $\gamma_i = 1$ , first for strange and next, light quarks. We also observe that allowing for  $\lambda_s \neq 1$  does not lead to an improvement in statistical significance, since the data is compatible with this value expected for the deconfined QGP. Similar systematic study has also been completed for the Pb–Pb system,<sup>45</sup> reconfirming the need to use  $\gamma_i \neq 1$  in the data analysis.

The errors in the results shown in table 1, and in results that follow below, are one standard deviation errors arising from the propagation of the experimental measurement error. However, these errors are meaningful only when the theoretical model describes the data well, as is the case for last entry line in table 1 when we allow light quark chemical nonequilibrium,  $\gamma_q \neq 1$ .

Table 1. Statistical parameters obtained from fits of S–Au/W/Pb data without enforcing strangeness conservation, and not considering flow effect — only compatible particle ratios were considered. Asterisk (\*) means a fixed (input) value. See text for an explanation of result errors.

$T_f$ [MeV]	$\lambda_q$	$\lambda_s$	$\gamma_s$	$\gamma_q$	$\chi_T^2/\text{dof}$
$145 \pm 3$	$1.52 \pm 0.02$	1*	1*	1*	17
$144 \pm 2$	$1.52 \pm 0.02$	$0.97 \pm 0.02$	1*	1*	18
$147 \pm 2$	$1.48 \pm 0.02$	$1.01 \pm 0.02$	$0.62 \pm 0.02$	1*	2.4
$144 \pm 3$	$1.49 \pm 0.02$	$1.00 \pm 0.02$	$0.73 \pm 0.02$	$1.22 \pm 0.06$	0.90

### 3. Strange Hadron Data Analysis

#### 3.1. Particle yields

The available compatible particle yield ratios (excluding presently  $\Omega$  and  $\bar{\Omega}$ , see subsection 3.4) are listed in table 2, top section from the experiment WA97, for  $p_\perp > 0.7$  GeV, within a narrow  $\Delta y = 0.5$  central rapidity window. Further below are shown results from the large acceptance experiment NA49, extrapolated by the collaboration to full  $4\pi$  phase space coverage. We first fit 11 experimental results shown in table 2, and then turn to include also the  $m_\perp$ -slope into this consideration, and thus have 12 data points. The total error  $\chi_T^2$  for the four result columns is shown at the bottom of this table along with the number of data points ‘ $N$ ’, parameters ‘ $p$ ’ used and (algebraic) redundancies ‘ $r$ ’ connecting the experimental results. For  $r \neq 0$  it is more appropriate to quote the total  $\chi_T^2$ , with a initial qualitative statistical relevance condition  $\chi_T^2/(N - p) < 1$ .

The first theoretical columns refer to results without collective velocity  $v_c$  (subscript 0) the three other were allowing for  $v_c$  (subscript  $v_c$ ). In column three, superscript ‘sb’ means that  $\lambda_s$  is fixed by strangeness balance and, in column four, superscript ‘sc’ means that  $\gamma_q = \gamma_q^c = e^{m_\pi/2T_f}$ , that is  $\gamma_q$  is fixed by its upper limit, the pion condensation point. All results shown account for slightly higher value of the ratio  $h^-/B$  recently reported<sup>36</sup>;  $B$  is here the number of baryon participants and  $h^- = \pi^- + K^- + \bar{p}$  is the yield of stable negative hadrons comprising as indicated pions, kaons and antiprotons.

First we note that all columns in table 2 represent physically acceptable result for the Pb–Pb collision system:

- a) presence of collective flow (three last columns) leads to very similar compatible particle ratios, even though improvement of  $\chi_T$  occurs when  $v_c \neq 0$  is allowed for;
- b) the highest confidence result is found just when the light quark phase space occupancy assumes a value at below the pion condensation point;
- c) strangeness conservation (enforced in second last column) is naturally present, enforcing it does not change in any way the results for particle multiplicities.

Allowing radial flow not only improves the capability to describe the data, but it allows us to study  $m_\perp$  particle spectra, which offer another independent measure of flow, and confirm the value of  $v_c$  — when considering  $v_c$  along with  $T_\perp$ , the



Table 2. WA97 (top) and NA49 (bottom) Pb–Pb 158A GeV particle ratios compared with theoretical results, see text for explanation.

Ratios	Ref.	Exp. Data	Pb  <sub>0</sub>	Pb  <sub>v</sub>	Pb  <sub>v</sub> <sup>sb</sup>	Pb  <sub>v</sub> <sup>sc</sup>
$\Xi/\Lambda$	64	$0.099 \pm 0.008$	0.104	0.103	0.105	0.103
$\bar{\Xi}/\bar{\Lambda}$	64	$0.203 \pm 0.024$	0.214	0.208	0.209	0.206
$\bar{\Lambda}/\Lambda$	64	$0.124 \pm 0.013$	0.124	0.125	0.124	0.125
$\bar{\Xi}/\Xi$	64	$0.255 \pm 0.025$	0.256	0.252	0.248	0.251
$\frac{(\bar{\Xi}+\Xi)}{(\Lambda+\bar{\Lambda})}$	66	$0.13 \pm 0.03$	0.126	0.122	0.124	0.122
$K_s^0/\phi$	62	$11.9 \pm 1.5$	14.2	13.3	13.0	13.4
$K^+/K^-$	63	$1.80 \pm 0.10$	1.80	1.82	1.78	1.83
$p/\bar{p}$	61	$18.1 \pm 4.$	17.3	16.7	16.6	16.6
$\bar{\Lambda}/\bar{p}$	67	$3. \pm 1.$	2.68	2.11	2.11	2.11
$K_s^0/B$	68	$0.183 \pm 0.027$	0.181	0.181	0.163	0.188
$h^-/B$	36	$1.97 \pm 0.1$	1.96	1.97	1.97	1.96
$\chi_T^2$			3.6	2.5	3.2	2.6
$N; p; r$			11;5;2	12;6;2	12;5;2	12;5;2

 Table 3. Experimental and theoretical  $m_\perp$  spectra inverse slopes  $T_{th}$ . Left Pb–Pb results from experiment WA97<sup>25,21</sup>; right S–W results from WA85.<sup>65</sup>

	$T_\perp^{Pb}$ [MeV]	$T_{th}^{Pb}$ [MeV]	$T_\perp^S$ [MeV]	$T_{th}^S$ [MeV]
$T^{K^0}$	$230 \pm 2$	241	$219 \pm 5$	215
$T^\Lambda$	$289 \pm 3$	280	$233 \pm 3$	236
$T^{\bar{\Lambda}}$	$287 \pm 4$	280	$232 \pm 7$	236
$T^\Xi$	$286 \pm 9$	298	$244 \pm 12$	246
$T^{\bar{\Xi}}$	$284 \pm 17$	298	$238 \pm 16$	246

inverse slope of the  $m_\perp$  spectra, we have one parameter and several spectral inverse slopes of particles considered. However, we will in the first instance assume that we have just one additional data point and we proceeded as follows: for a given pair of values  $T_f$  and  $v_c$  we evaluate the resulting  $m_\perp$  particle spectrum and analyze it using the spectral shape and kinematic cuts employed by the experimental groups. Once we find values of  $T_f$  and  $v_c$ , we study again the inverse slopes of individual particle spectra and obtain an acceptable agreement with the experimental  $T_\perp^j$  as shown in left section of table 3. We have considered in the same framework the S-induced reactions, and the right section of table 3 shows also a good agreement with the WA85 experimental data.<sup>65</sup>

We have updated the experimental Pb–Pb results shown in table 3 with the current high precision results.<sup>21</sup> However, the theoretical results shown were obtained earlier for slightly different results with larger error bars, and we hope to reevaluate these results in the near future. To model these slopes theoretically, one needs to remember that the vast majority of  $\Lambda$  and  $\bar{\Lambda}$  is a decay product of  $\Sigma^0$  and  $\bar{\Sigma}^0$ ,  $\Lambda^*$  and  $\bar{\Lambda}^*$  and  $\Xi$  and  $\bar{\Xi}$ . Consequently, given the precision of the (inverse) slopes presented, in order to model the  $\Lambda$  and  $\bar{\Lambda}$  spectra one will need to consider the effect

of hadron cascading, which introduces uncertainty arising from a dependence on unmeasured yields. However, given the current availability of quite precise  $\Xi$  and  $\bar{\Xi}$  slopes, and the fact that these particles are rarely decay products of other hadronic resonances, we will in future use these slopes as the spectral data point input in the data analysis studies. As result, we anticipate a slight reduction in the collective velocity within the errors shown below.

### 3.2. Chemical freeze-out properties

The six parameters  $(T_f, v_c, \lambda_q, \lambda_s, \gamma_q, \gamma_s)$  describing the particle abundances are shown in the top section of table 4. We also show in the last column the best result for S-induced reactions, where the target has been W/Au/Pb.<sup>44</sup> All results shown in table 4 have convincing statistical confidence level. For the S-induced reactions the number of redundancies  $r$  shown in the heading of the table 4 is large, since the same data comprising different kinematic cuts has been included in the analysis.

Within error, the freeze-out temperature  $T_f \simeq 143 \pm 3$  MeV, seen in table 4, is the same for both the S- and Pb-induced reactions, even though the chemical phase space occupancies differ greatly. Such a behavior is expected in view of the similarity of the energy content in the collision in both reaction systems, but greatly differing collision geometry. We find that the variation in the shape of particle  $m_\perp$ -spectra is fully explained by a change in the collective velocity, which rises from  $v_c^S = 0.49 \pm 0.02$  to  $v_c^{Pb} = 0.54 \pm 0.04 \simeq 1/\sqrt{3} = 0.577$ . The value of light quark fugacity  $\lambda_q$  implies that baryochemical potential is  $\mu_B^{Pb} = 203 \pm 5 > \mu_B^S = 178 \pm 5$  MeV. As in S-induced reactions where  $\lambda_s = 1$ , now in Pb-induced reactions, a value  $\lambda_s^{Pb} \simeq 1.1$  characteristic for a source of freely movable strange quarks with balancing strangeness, *i.e.*,  $\bar{\lambda}_s = 1$ , is obtained, see Eq. (13).

Further evidence for low chemical freeze-out temperature is contained in the  $m_\perp$ -particle spectra considered in subsection 3.1. Our approach offers a natural understanding of the equality of the  $m_\perp$ -slopes of the strange baryons and antibaryons considered which arises because within the sudden hadronization model both these particles emerge free-streaming from QGP. In the hadron based microscopic simulations this behavior of  $m_\perp$ -slopes of baryons and antibaryons arises from fine-tuning of the particle-dependent freeze-out times.<sup>69</sup> On the other hand, in such a microscopic study one finds in view of the small reaction cross sections that  $\Omega$  and  $\bar{\Omega}$  could freeze out somewhat sooner than the other hadrons, and thus would have a softer spectrum as also confirmed in direct hadronization simulations.<sup>70</sup> We will return to this point just below. The reader should keep in mind that since we find a rather low chemical freeze-out temperature, and can explain the  $m_\perp$  spectra well based on this value, the implied kinetic (collision) freeze-out temperature must be rather similar to the chemical freeze-out.

In the bottom section of table 4, we also see the energy and entropy content per baryon. The energy per baryon seen in the emitted hadrons is nearly equal to the available specific energy of the collision (8.6 GeV for Pb-Pb, 8.8–9 GeV for S-Au/W/Pb). This implies that the fraction of energy deposited in the central fireball

Table 4. In heading, we present the total quadratic relative error  $\chi^2_{\text{T}}$ , number of data points  $N$ , parameters  $p$  and redundancies  $r$ ; in the upper section: statistical model parameters which best describe the experimental results for Pb–Pb data, and in last column for S–Au/W/Pb data presented in Ref. <sup>44</sup>. Bottom section: specific energy, entropy, anti-strangeness, net strangeness of the full hadron phase space characterized by these statistical parameters. In column two, we fix  $\lambda_s$  by requirement of strangeness conservation, and in column three, we fix  $\gamma_q$  at the pion condensation point  $\gamma_q = \gamma_q^c$ .

	Pb  <sub>v</sub>	Pb  <sub>v</sub> <sup>sb</sup>	Pb  <sub>v</sub> <sup>sc</sup>	S  <sub>v</sub>
$\chi^2_{\text{T}}; N; p; r$	2.5; 12; 6; 2	3.2; 12; 5; 2	2.6; 12; 5; 2	6.2; 16; 6; 6
$T_f$ [MeV]	142 ± 3	144 ± 2	142 ± 2	144 ± 2
$v_c$	0.54 ± 0.04	0.54 ± 0.025	0.54 ± 0.025	0.49 ± 0.02
$\lambda_q$	1.61 ± 0.02	1.605 ± 0.025	1.615 ± 0.025	1.51 ± 0.02
$\lambda_s$	1.09 ± 0.02	1.10*	1.09 ± 0.02	1.00 ± 0.02
$\gamma_q$	1.7 ± 0.5	1.8 ± 0.2	$\gamma_q^{c*} = e^{m_\pi/2T_f}$	1.41 ± 0.08
$\gamma_s/\gamma_q$	0.79 ± 0.05	0.80 ± 0.05	0.79 ± 0.05	0.69 ± 0.03
$E_f/B$	7.8 ± 0.5	7.7 ± 0.5	7.8 ± 0.5	8.2 ± 0.5
$S_f/B$	42 ± 3	41 ± 3	43 ± 3	44 ± 3
$s_f/B$	0.69 ± 0.04	0.67 ± 0.05	0.70 ± 0.05	0.73 ± 0.05
$(\bar{s}_f - s_f)/B$	0.03 ± 0.04	0*	0.04 ± 0.05	0.17 ± 0.05

must be nearly (within 10%) the same as the fraction of baryon number. The small reduction of the specific entropy in Pb–Pb compared to the lighter S–Au/W/Pb system maybe driven by the greater baryon stopping in the larger system, also seen in the smaller energy per baryon content. Both collision systems freeze out at the same energy per unit of entropy,

$$E/S = 0.185 \text{ GeV}.$$

There is a loose relation of this universality in the chemical freeze-out condition with the suggestion made recently that particle freeze-out occurs at a fixed energy per baryon for all physical systems,<sup>71</sup> considering that the entropy content is related to particle multiplicity. The overall high specific entropy content we find agrees well with the entropy content evaluation we made earlier for the S–Pb case.<sup>40</sup> The high entropy content is observed in the final hadron state in terms of enhanced pion yield. Thus the ratio of  $K^+/\pi^+$  is combines these two effects and is not a good indicator of new physics, even though this relatively simple observable continues to attract attention.<sup>72</sup> It would have been more useful if systematic studies of strangeness production and enhancement were to offer as result of their analysis the strangeness yields per participating baryon number.

The large values of  $\gamma_q > 1$ , seen in table 4, imply as discussed earlier that there is phase space over-abundance of light quarks, which receives contribution from, *e.g.*, gluon fragmentation at QGP breakup.  $\gamma_q$  assumes in the data analysis a value near to where pions could begin to condense,<sup>55</sup> Eq. (3). This result is consistent with the expectations for hadronization of an entropy rich quark gluon plasma, as we discussed above in subsection **2.3**. We found by studying the ratio  $h^-/B$  separately from other experimental results that the value of  $\gamma_q \simeq \gamma_q^c$  is fixed consistently and

independently both, by the negative hadron ( $h^-$ ), and the strange hadron yields. The unphysical range  $\gamma_q > \gamma_q^c \simeq 1.63$  can arise (see column  $\text{Pb|Pb}^{Sb}$ ) since, up to this point, we had used only a first quantum (Bose/Fermi) correction. However, when Bose distribution for pions is implemented, which requires the constraint  $\gamma_q \leq \gamma_q^c$ , we obtain practically the same results, as shown in the third column of table 4.

### 3.3. Strangeness enhancement

We show, in the bottom section of table 4, the specific strangeness content,  $s_f/B$  along with specific strangeness asymmetry  $(\bar{s}_f - s_f)/B$  seen in the hadronic particles emitted. In the data analysis the requirement that the number of  $s$  and  $\bar{s}$  quarks in hadrons is equal is in general not enforced. We see that in lower portion of table 4 that this result is found automatically for the symmetric Pb–Pb collision system. However, a 3.5 s.d. effect is seen in the asymmetrical S–Au/W/Pb system. Though the errors which we derive from the experimental data are small, there could be in this asymmetric system a considerable systematic experimental error due to data extrapolations made in presence of a significant spectator matter component, coupled with theoretical error from the varying CM-rapidity. On the other hand, the consistency of the Pb–Pb and S–Au/W/Pb results suggest that this asymmetry is possibly a real effect, thus the unseen balance of strangeness could be hidden in a residual (strange) quark matter nugget, which is escaping detection. Such strangelets could in principle form, since in the hadronization of the S–Au/W/Pb deconfined system the hadron phase space is asymmetric, which leads to strangeness distillation.<sup>73,74,75,76</sup>

One of the important quantitative results of this analysis is shown in the bottom section of table 4: the high yield of strangeness per baryon,  $s_f/B \simeq 0.7$ . We now proceed to verify if this yield is in agreement with the predictions made over the past 20 years. Perhaps more by chance than design, this analysis result is in agreement with the first calculations of strangeness production employing perturbative QCD,<sup>12</sup> where the value  $N_s/B = n_s/\nu = 0.7$  is reached for the plasma temperature of 300 MeV as shown there in Fig. 3. Since, considerably more refined methods have been developed,<sup>16</sup> and these are in excellent agreement with results of the analysis of experimental results. In view of the high precision reached in this data analysis, we have recomputed the theoretical yield taking for the QCD parameters values generally accepted today:  $\alpha_s(M_Z) = 0.118$  and  $m_s(1\text{GeV}) = 200$  MeV, corresponding to  $m_s(M_Z) = 90$  MeV.

In table 5, we summarize for three collision systems we consider S–Au/W/Pb, Ag–Ag, Pb–Pb the key input parameters used in computing the result for  $N_s/B$  shown below in Fig. 3. The first entry line gives the central collision participant numbers for the three systems considered. Next, in table 5, we see the initial temperature  $T_{\text{ch}}$  which the evaluation of strangeness production requires as input.  $T_{\text{ch}}$  is the temperature at the time when light quarks and gluons reach equilibrium. To obtain this value, we compute the collisional pressure and set it equal to thermal pressure at the time the fireball begins to expand.<sup>16,20</sup> To do this we need the (mo-

Table 5: Input to the strangeness production computation in QGP.

		S–Au/W/Pb	Ag–Ag	Pb–Pb
participants	$B$	90	180	360
$q, G$ equilibration	$T_{\text{ch}}[\text{MeV}]$	260	280	320
stopping	$\eta$	52%	54%	57%
scale expansion velocity	$v_c$	$0.49c$	$0.52c$	$0.54c$

momentum, energy) stopping fractions  $\eta$  here taken from NA35/NA49 experimental results,<sup>35</sup> (except for interpolation for Ag–Ag, the dotted line in Fig. 3). The last line in table 5 addresses the expansion dynamics we use: we employ the observed freeze-out expansion velocity  $v_c$  as given in the top section of table 4. We assume that each local volume expands its size scale  $R$  at this local velocity, and we consider the process to be entropy conserving, hence we use  $R^3 T^3 = \text{Const.}$  to obtain the time dependence of local fireball temperature.

We obtain the result for  $N_s/B$  shown in Fig. 3, as function of the specific energy available in the fireball  $E/B$ , for the three collision systems S–Au/W/Pb (short-dashed line), Ag–Ag (long dashed) and Pb–Pb (solid line). Since we compute the initial temperature from the collision energy our approach allows us to extrapolate as function of  $E/B$ , assuming that the stopping fraction for the collisional pressure is known. When we keep the stopping fraction constant and as given at the 160–200A GeV collision energy, we find the results shown in Fig. 3. However, a constant stopping underestimates the initial temperature at lower collision energy, where we would expect higher stopping, and it overestimates the initial temperature at higher collision energies, where we would expect smaller stopping, thus we believe that the slope of the result we present in Fig. 3 is too steep. We will be able to improve on this result after the behavior of stopping as function of collision energy has been understood.

In Fig. 3, the solid square is the result of the analysis for S–Au/W/Pb system, and open square for Pb–Pb as shown in the lower section of table 4. We note that the reason that the available energy  $E/B$  in the fireball is the dominant parameter controlling strangeness yield is the cancellation of effect of higher initial temperature in the larger, more stopping systems, by the faster explosion of such a system, which leaves less time for strangeness production. We note that even though we did not analyze here the S–S system, for which case we would need to adapt the method to allow significant longitudinal flow, it is understood that the available fireball energy and strangeness content per baryon is higher in S–S 200A GeV interactions,<sup>60</sup> consistent with the results shown in Fig. 3.

This high strangeness yield corresponds to (above) equilibrium abundance phase space occupancy in hadronization. In the top section of table 4, the ratio  $\gamma_s/\gamma_q \simeq 0.8$ , which corresponds (approximately) to the parameter  $\gamma_s$  when  $\gamma_q = 1$  has been assumed. We observe that  $\gamma_s^{\text{Pb}} > 1$ . This strangeness over-saturation effect could

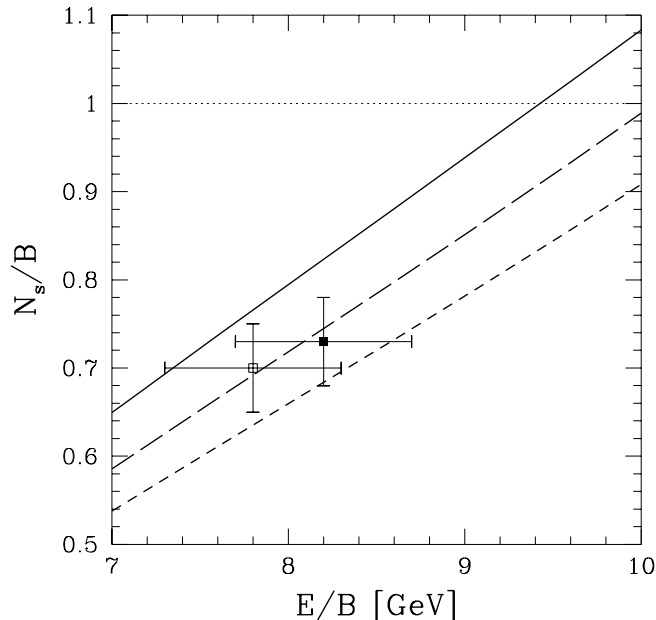


Fig. 3. QGP fireball specific per baryon strangeness abundance as function of  $E/B$  energy per baryon in the fireball, for running  $\alpha_s(M_Z) = 0.118$  and  $m_s(1\text{GeV}) = 200$  MeV, corresponding to  $m_s(M_Z) = 90$  MeV. Solid lines: for Pb–Pb, stopping 57% and 360 participants, long-dashed lines: for Ag–Ag, stopping 54% and 180 participants, short-dashed lines: for S–Au/W/Pb stopping 52% and 90 participants in QGP fireball. The solid square is the result of an analysis for S–Au/W/Pb 200A GeV reaction system, and open square for Pb–Pb at 158A GeV, as shown in the lower section of table 4.

arise from the effect of gluon fragmentation combined with early chemical equilibration in the QGP,  $\gamma_s(t < t_f) \simeq 1$ . The ensuing rapid expansion preserves this high strangeness yield, and thus we find the result  $\gamma_s > 1$ , as we reported in Ref. <sup>16</sup>. This high phase space occupancy is one of the requirements for the enhancement of multi-strange (anti)baryon production, which is an important hadronic signal of QGP phenomena.<sup>11</sup>

We compare this result of data analysis, in quantitative manner, with the theoretical computation of  $\gamma_s$  which is easily obtained from the above study of total strangeness production, as we only need to divide the total momentary strangeness yield by the expected equilibrium abundance, for which we choose to consider ideal gas of strange quarks with QCD running mass  $m_s(\mu = 5.5T)$ . The factor 5.5 converts the value of  $T$  into the appropriate scale  $\mu$  of energy at which the kinetic equilibrium distribution is formed, and we note that  $m_s(T = 182 \text{ MeV}) = 200 \text{ MeV}$ . The effect of QCD running influences the agreement between theory and experiment at the level of 10–15%. The result is shown in figure 4, right as function of time  $t$  for the 160–200A GeV collision systems and left as function of temperature  $T$ . Horizontal dotted line refers to equilibrium phase space occupancy, and the vertical

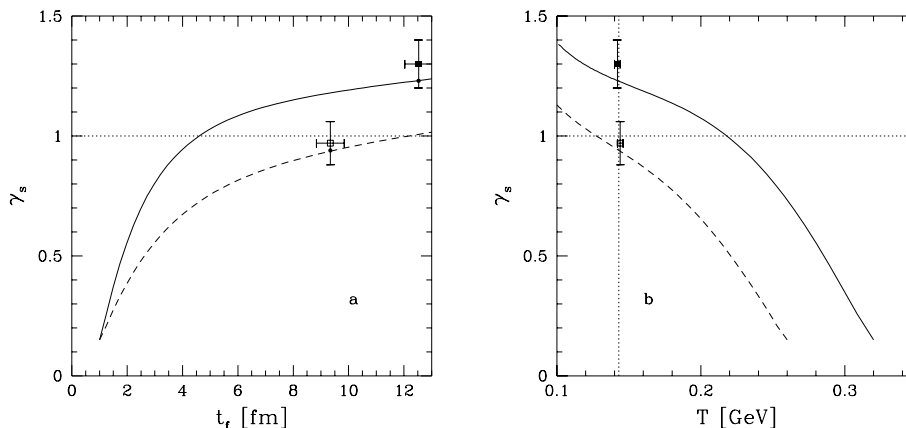


Fig. 4. Evolution of strangeness phase space occupancy  $\gamma_s$ , **a)** as function of time  $t$  (on left) and **b)** as function of temperature  $T$  (on right) for the 160–200A GeV collision systems. For further explanation see legend to figure 3 and text.

line indicates expected freeze-out condition at  $T_f = 143$  MeV.

Solid dots in figure 4**a)** show where this freeze-out temperature occurs as function of time  $t$ . The analysis point uncertainty in freeze-out time is obtained assuming that, in isentropic evolution, size scale  $R$  and temperature satisfy  $RT = \text{Const.}$ , and thus with  $v_c = dR/dt|_f$  we find:

$$\Delta t = -\frac{R_f}{v_c T} \Delta T. \quad (23)$$

The chemical freeze-out occurs at about 10 fm/c and 13 fm/c, after onset of the collision, allowing for about 1 fm/c initial time  $\tau_{\text{ch}}$  for the two systems S–Au/W/Pb and Pb–Pb respectively. Considering that the expansion velocity has been 0.5c and 0.64c respectively we obtain an estimate of the chemical freeze-out radius  $R_f^S \simeq 5$  fm and  $R_f^{\text{Pb}} \simeq 8$  fm, the latter value is in excellent agreement with the discussion of the Coulomb effect presented in section 2.2.

### 3.4. The Omega riddle

The QGP formation and sudden disintegration model we have described above has natural limitations. When we attempt to describe within this approach most rarely produced particles, there is the potential for under-prediction of experimental results, which could receive contributions from other more effective production mechanisms. In this context, the most rarely produced hadron is the triply strange  $\Omega(sss)$  and  $\bar{\Omega}(\bar{s}\bar{s}\bar{s})$  which are the heaviest stable hadrons,  $M_\Omega = 1672$  MeV. The phase space for  $\Omega$  is more than 10 times smaller than that for  $\Xi$  at the conditions of chemical freeze-out we have obtained.  $\Omega$  and  $\bar{\Omega}$  production pattern can thus be altered by processes not implemented in the one stage fireball model used to analyze the data.

Table 6: Pb–Pb 158A GeV particle ratios involving  $\Omega$  and  $\bar{\Omega}$ , compared to theoretical expectations for  $T_f = 143$  MeV. \* reminds us that statistical parameters are fixed by other particle yields. Last column presents results allowing a 11%  $\Xi$  and  $\bar{\Xi}$  shadow, see text for details.

Ratios	Ref.	Exp. Data	$v = 0$	$v_c$	11 %
$\Omega/\Xi$	64	$0.192 \pm 0.024$	0.078*	0.077*	0.186
$\bar{\Omega}/\bar{\Xi}$	78	$0.27 \pm 0.06$	0.17*	0.18*	0.28
$\bar{\Omega}/\Omega$	64	$0.38 \pm 0.10$	0.57*	0.60*	0.38
$\frac{(\Omega+\bar{\Omega})}{(\Xi+\bar{\Xi})}$	78	$0.20 \pm 0.03$	0.10*	0.10*	0.206

When we attempted to describe along with the other hadrons the yields of  $\Omega$  and  $\bar{\Omega}$  within the single stage freeze-out model, we indeed have discovered considerable loss of physical significance.<sup>45</sup> Already for the S–Au/W/Pb case, we have found that a more reliable description of the data arises if we did not consider the qualitative Omega yields available.<sup>44</sup> For the parameters as reported, we find in the Pb–Pb reactions that we under-predict the  $\Omega$  and  $\bar{\Omega}$  yields by about factor 2. The experimental results are shown in the first three columns of table 6 and the theoretical yield computed using the Fermi-2000 model with parameters fixed by other particle abundances are shown in columns 4 and 5: we see that the presence of radial flow ( $v = v_c$ ) has a minimal impact on the relative yields, compared to the case without radial flow ( $v = 0$ ). To put this result into proper perspective, consider that we find within the sudden hadronization of QGP with uncorrelated strange quarks in the deconfined phase an enhancement of  $\Omega$  and  $\bar{\Omega}$  yields ‘only’ by factor 10 as compared to what is expected from extrapolation of p–A reactions. However, the experiment reports an enhancement by factor 15–20. Such a ‘failure’ is in fact confirming the early expectations that  $\Omega$  and  $\bar{\Omega}$  yields are the best signature of deconfinement, considering the possibility of strange quark clustering.<sup>11</sup> In fact it is a bit surprising how well this early prediction works, and this requires further study to understand more precisely what exactly this means.

Several groups have noted, studying the microscopic evolution of  $\Omega$  and  $\bar{\Omega}$ , that due to low reaction cross section they decouple from hadron background somewhat sooner than all the other hadrons.<sup>69,70</sup> An early chemical freeze-out would impact statistical yields of  $\Omega$  and  $\bar{\Omega}$  greatly. To augment the  $\Omega$  and  $\bar{\Omega}$  yields by factor  $k$ , it is sufficient to take an incrementally  $\delta T$  higher freeze-out temperature, as determined from study of the  $\Omega$  phase space:

$$\delta T \simeq T \frac{\ln k}{M_\Omega/T}. \quad (24)$$

Thus in order to increase the yields by a factor 2 the  $\Omega$  and  $\bar{\Omega}$  freeze-out would need to occur at  $T_\Omega = 150$  MeV rather than at  $T_f = 143$  MeV. Since the temperature drops as the explosion of the fireball develops, this higher freeze-out temperature



means an earlier in time freeze-out.

Even if the required staging in time of hadron production is apparently small, a consistent picture requires fine-tuning and it seems unnatural, considering that all the other particles are perfectly consistent with just one sudden freeze-out condition. Pursuing other alternatives, we note that  $\Omega$  and  $\bar{\Omega}$  enhancement is caused by strangeness pre-clustering in the deconfined phase which would enhance multi-strange hadrons, but most prominently and noticeable enhance the phase space suppressed  $\Omega$  and  $\bar{\Omega}$ . In this context, it is interesting to note that the missing yield is not symmetric: as seen in table 6 we miss in relative terms more  $\Omega$  than  $\bar{\Omega}$ . Interestingly, the missing yield is exactly proportional to the yield of  $\Xi$  and  $\bar{\Xi}$  and the best description of all particle yields, including all  $\Omega$  and  $\bar{\Omega}$  is arrived at describing what is missing as proportional (11 %) to the  $\Xi$  and  $\bar{\Xi}$  yield, this is shown in the last column ‘11 %’ of table 6. It is now easy to propose a model that would lead just to this result: there are colored di-strange quarks clusters at hadronization and when their color strings break  $\Xi$  and  $\Omega$  are produced. This imprints a ‘shadow’ of  $\Xi$  and  $\bar{\Xi}$  in the  $\Omega$  and  $\bar{\Omega}$ -abundance. While this works for  $\Omega$  and  $\bar{\Omega}$ , we find that this mechanism is not compatible with the other particle abundances, in other words a similar ‘shadow’ of  $\Lambda$  and  $\bar{\Lambda}$  in the  $\Xi$  and  $\bar{\Xi}$  channel seems unacceptable. Thus this mechanism would work only if pairing of strange quarks would be significant near to phase transition. Current models of ‘color super conductivity’ support such a clustering mechanism for additional  $\Omega$  and  $\bar{\Omega}$  enhancement, though detailed studies are still in progress.<sup>79</sup>

We have also explored the possibility that unknown  $\Omega^*$  and  $\bar{\Omega}^*$  resonances contribute to the  $\Omega$  and  $\bar{\Omega}$  yield, but we were not able to find a good set of parameters for these hypothetical resonances. Moreover, this hypothesis implies a baryon–antibaryon symmetric contribution in the sense that both  $\Omega$  and  $\bar{\Omega}$  yields are multiplied by the same factor. However, the missing yield is clearly also baryon–antibaryon asymmetric — thus despite several ad-hoc parameters the model description remains poor.

We note that earlier statistical descriptions of  $\Omega$  and  $\bar{\Omega}$  yields have not been sensitive to the problems we described.<sup>53,77</sup> In fact as long as the parameter  $\gamma_q$  is not considered, it is not possible to describe the experimental data at the level of precision that would allow recognition of the  $\Omega$  and  $\bar{\Omega}$  yield as a problem for the statistical Fermi phase space model.

#### 4. Kinetic Strangeness Production

In some computational details, the methods to describe strangeness production differ.<sup>80,81,82,83</sup> This leads to different expectations regarding chemical equilibration of quark flavor at RHIC energies, with some authors finding marginal at best chemical equilibration. We therefore develop in more detail the computational approach which is consistent with the SPS-energy scale results discussed in previous sections.<sup>83</sup> One important difference to the earlier work is that the two loop level running of QCD parameters for both coupling strength  $\alpha_s$  and strange quark mass

$m_s$  is used.  $\alpha_{M_Z} = 0.118$  is assumed as determined at the  $\mu = M_{Z^0}$  energy scale. Another improvement is that an entropy conserving explosive flow of matter is incorporated directly into the dynamical equations describing the evolution of strangeness phase space occupancy. This approach is entailing significant cancellations in the dynamical equations and the only model dependence on matter flow which remains is the relationship between the local temperature and local proper time. In consequence, a relatively simple and physically transparent model for the evolution of the phase space occupancy  $\gamma_s$  of strange quarks in the expanding QGP can be studied.

We use two assumptions of relevance for the results we obtain:

- the kinetic (momentum distribution) equilibrium is reached faster than the chemical (abundance) equilibrium<sup>84,85</sup>;
- gluons equilibrate chemically significantly faster than strangeness.<sup>86</sup>

The first assumption allows us to study only the chemical abundances, rather than the full momentum distribution, which simplifies greatly the structure of the master equations; the second assumption allows us to consider the evolution of the strangeness population only after an initial time  $\tau_{\text{ch}}$  period has passed:  $\tau_{\text{ch}}$  is the time required for the development to near chemical equilibrium of the gluon population, and the corresponding temperature  $T_{\text{ch}}$  is the initial condition we need to compute the evolution of strangeness. Aside of  $T_{\text{ch}}$ , the strange quark mass  $m_s$  introduces the greatest uncertainty that enters strangeness yield calculations based on resummed perturbative QCD rates.<sup>87</sup> The overpopulation of the strangeness phase space, seen before in section 3 in SPS data, arises in particular for  $T_{\text{ch}} > 250$  MeV and values of strange quark mass  $m_s(1\text{GeV}) \simeq 200 \pm 20$  MeV.

In view of these assumptions the phase space distribution  $f_s$  can be characterized by a local temperature  $T(\vec{x}, t)$  of a (Boltzmann) equilibrium distribution  $f_s^\infty$ , with normalization set by a phase space occupancy factor:

$$f_s(\vec{p}, \vec{x}; t) \simeq \gamma_s(T) f_s^\infty(\vec{p}; T). \quad (25)$$

Eq. (25) invokes in the momentum independence of  $\gamma_s$  the first assumption. More generally, the factor  $\gamma_i$ ,  $i = g, q, s, c$ , allows the local density of gluons, light quarks, strange quarks and charmed quarks, respectively to evolve independently of the local momentum shape. With variables  $(t, \vec{x})$  referring to an observer in the laboratory frame, the chemical evolution can be described by the strange quark current non-conservation arising from strange quark pair production described by a Boltzmann collision term:

$$\begin{aligned} \partial_\mu j_s^\mu \equiv \frac{\partial \rho_s}{\partial t} + \frac{\partial \vec{v} \rho_s}{\partial \vec{x}} &= \frac{1}{2} \rho_g^2(t) \langle \sigma v \rangle_T^{gg \rightarrow s\bar{s}} \\ &+ \rho_q(t) \rho_{\bar{q}}(t) \langle \sigma v \rangle_T^{q\bar{q} \rightarrow s\bar{s}} - \rho_s(t) \rho_{\bar{s}}(t) \langle \sigma v \rangle_T^{s\bar{s} \rightarrow gg, q\bar{q}}. \end{aligned} \quad (26)$$

The factor 1/2 avoids double counting of gluon pairs. The implicit sums over spin, color and any other discrete quantum numbers are combined in the particle density  $\rho = \sum_{s,c,\dots} \int d^3p f$ , and we have also introduced the momentum averaged

production/annihilation thermal reactivities (also called ‘rate coefficients’):

$$\langle \sigma v_{\text{rel}} \rangle_T \equiv \frac{\int d^3 p_1 \int d^3 p_2 \sigma_{12} v_{12} f(\vec{p}_1, T) f(\vec{p}_2, T)}{\int d^3 p_1 \int d^3 p_2 f(\vec{p}_1, T) f(\vec{p}_2, T)}. \quad (27)$$

$f(\vec{p}_i, T)$  are the relativistic Boltzmann/Jüttner distributions of two colliding particles of momentum  $p_i$ ,  $i = 1, 2$ .

The current conservation used above in the laboratory ‘Eulerian’ formulation can also be written with reference to the individual particle dynamics in the so called ‘Lagrangian’ description: consider  $\rho_s$  as the inverse of the small volume available to each particle. Such a volume is defined in the local frame of reference for which the local flow vector vanishes  $\vec{v}(\vec{x}, t)|_{\text{local}} = 0$ . The considered volume  $\delta V_l$  being occupied by small number of particles  $\delta N$  (*e.g.*,  $\delta N = 1$ ), we have:

$$\delta N_s \equiv \rho_s \delta V_l. \quad (28)$$

The left hand side (LHS) of Eq. (26) can be now written as:

$$\frac{\partial \rho_s}{\partial t} + \frac{\partial \vec{v} \rho_s}{\partial \vec{x}} \equiv \frac{1}{\delta V_l} \frac{d \delta N_s}{dt} = \frac{d \rho_s}{dt} + \rho_s \frac{1}{\delta V_l} \frac{d \delta V_l}{dt}. \quad (29)$$

Since  $\delta N$  and  $\delta V_l dt$  are L(orentz)-invariant, the actual choice of the frame of reference in which the right hand side (RHS) of Eq. (29) is studied is irrelevant and we drop henceforth the subscript  $l$ .

We can further adapt Eq. (29) to the dynamics we pursue: we introduce  $\rho_s^\infty(T)$  as the (local) chemical equilibrium abundance of strange quarks, thus  $\rho = \gamma_s \rho_s^\infty$ . We evaluate the equilibrium abundance  $\delta N_s^\infty = \delta V \rho_s^\infty(T)$  integrating the Boltzmann distribution:

$$\delta N_s^\infty = [\delta V T^3] \frac{3}{\pi^2} z^2 K_2(z), \quad z = \frac{m_s}{T}. \quad (30)$$

We will below use:  $d[z^\nu K_\nu(z)]/dz = -z^\nu K_{\nu-1}$ , where  $K_\nu$  is the modified Bessel function of order  $\nu$ . The first factor on the RHS in Eq. (30) is a constant in time should the evolution of matter after the initial pre-thermal time period  $\tau_0$  be entropy conserving,<sup>88</sup> and thus  $\delta V T^3 = \delta V_0 T_0^3 = \text{Const.}$ . We now substitute in Eq. (29) and obtain

$$\frac{\partial \rho_s}{\partial t} + \frac{\partial \vec{v} \rho_s}{\partial \vec{x}} = \dot{T} \rho_s^\infty \left( \frac{d \gamma_s}{dT} + \frac{\gamma_s}{T} z \frac{K_1(z)}{K_2(z)} \right), \quad (31)$$

where  $\dot{T} = dT/dt$ . Note that, in Eq. (31), only a part of the usual flow-dilution term is left, since we implemented the adiabatic volume expansion, and study the evolution of the phase space occupancy in lieu of particle density. The dynamics of the local temperature is the only quantity we need to model.

We now return to study the collision terms seen on the RHS of Eq. (26). A related quantity is the (L-invariant) production rate  $A^{12 \rightarrow 34}$  of particles per unit time and space, defined usually with respect to chemically equilibrated distributions:

$$A^{12 \rightarrow 34} \equiv \frac{1}{1 + \delta_{1,2}} \rho_1^\infty \rho_2^\infty \langle \sigma_s v_{12} \rangle_T^{12 \rightarrow 34}. \quad (32)$$

The factor  $1/(1 + \delta_{1,2})$  is introduced to compensate double-counting of identical particle pairs. In terms of the L-invariant  $A$ , Eq. (26) takes the form:

$$\begin{aligned} \dot{T}\rho_s^\infty \left( \frac{d\gamma_s}{dT} + \frac{\gamma_s}{T} z \frac{K_1(z)}{K_2(z)} \right) &= \gamma_g^2(\tau) A^{gg \rightarrow s\bar{s}} + \\ &+ \gamma_q(\tau) \gamma_{\bar{q}}(\tau) A^{q\bar{q} \rightarrow s\bar{s}} - \gamma_s(\tau) \gamma_{\bar{s}}(\tau) (A^{s\bar{s} \rightarrow gg} + A^{s\bar{s} \rightarrow q\bar{q}}). \end{aligned} \quad (33)$$

Only weak interactions convert quark flavors, thus, on hadronic time scale, we have  $\gamma_{s,q}(\tau) = \gamma_{\bar{s},\bar{q}}(\tau)$ . Moreover, detailed balance, arising from the time reversal symmetry of the microscopic reactions, assures that the invariant rates for forward/backward reactions are the same, specifically

$$A^{12 \rightarrow 34} = A^{34 \rightarrow 12}, \quad (34)$$

and thus:

$$\begin{aligned} \dot{T}\rho_s^\infty \left( \frac{d\gamma_s}{dT} + \frac{\gamma_s}{T} z \frac{K_1(z)}{K_2(z)} \right) &= \gamma_g^2(\tau) A^{gg \rightarrow s\bar{s}} \left[ 1 - \frac{\gamma_s^2(\tau)}{\gamma_g^2(\tau)} \right] \\ &+ \gamma_q^2(\tau) A^{q\bar{q} \rightarrow s\bar{s}} \left[ 1 - \frac{\gamma_s^2(\tau)}{\gamma_q^2(\tau)} \right]. \end{aligned} \quad (35)$$

When all  $\gamma_i \rightarrow 1$ , the Boltzmann collision term vanishes, we have reached equilibrium.

As discussed, the gluon chemical equilibrium is thought to be reached at high temperatures well before the strangeness equilibrates chemically, and thus we assume this in what follows, and the initial conditions we will study refer to the time at which gluons are chemically equilibrated. Setting  $\lambda_g = 1$  (and without a significant further consequence for what follows, since gluons dominate the production rate, also  $\lambda_q = 1$ ), we obtain after a straightforward manipulation the dynamical equation describing the evolution of the local phase space occupancy of strangeness:

$$2\tau_s \dot{T} \left( \frac{d\gamma_s}{dT} + \frac{\gamma_s}{T} z \frac{K_1(z)}{K_2(z)} \right) = 1 - \gamma_s^2. \quad (36)$$

Here, we defined the relaxation time  $\tau_s$  of chemical (strangeness) equilibration as the ratio of the equilibrium density that is being approached, with the rate at which this occurs:

$$\tau_s \equiv \frac{1}{2} \frac{\rho_s^\infty}{(A^{gg \rightarrow s\bar{s}} + A^{q\bar{q} \rightarrow s\bar{s}} + \dots)}. \quad (37)$$

The factor  $1/2$  is introduced by convention in order for the quantity  $\tau_s$  to describe the exponential approach to equilibrium.

Eq. (36) is the final analytical result describing the evolution of phase space occupancy. Since one generally expects that  $\gamma_s \rightarrow 1$  in a monotonic fashion as function of time, it is important to appreciate that this equation allows the range  $\gamma_s > 1$ : when  $T$  drops below  $m_s$ , and  $1/\tau_s$  becomes small, the dilution term (2nd term on LHS) in Eq. (36) dominates the evolution of  $\gamma_s$ . In simple terms, the high

abundance of strangeness produced at high temperature over-populates the available phase space at lower temperature, when the equilibration rate cannot keep up with the expansion cooling. This behavior of  $\gamma_s$  has been shown for the SPS conditions allowing explosive transverse expansion in subsection 3.3. Since we assume that the dynamics of transverse expansion of QGP is similar at RHIC as at SPS, we obtain similar behavior for  $\gamma_s$  in section 5 below.

$\tau_s(T)$ , Eq. (37), has been evaluated using pQCD cross section and employing next to leading order running of both the strange quark mass and QCD-coupling constant  $\alpha_s$ .<sup>87</sup> We believe that this method produces a result for  $\alpha_s$  that can be trusted down to just below 1 GeV energy scale which is here relevant. We employ results obtained with  $\alpha_s(M_{Z^0}) = 0.118$  and  $m_s(1\text{ GeV}) = 200\text{ MeV}$ ; we have shown results with  $m_s(1\text{ GeV}) = 220\text{ MeV}$  earlier.<sup>83</sup> There is some systematic uncertainty due to the appearance of the strange quark mass as a fixed rather than running value in both, the chemical equilibrium density  $\rho_s^\infty$  in Eq. (37), and in the dilution term in Eq. (36). We use the value  $m_s(1\text{ GeV})$ , with the 1 GeV energy scale chosen to correspond to typical interaction scale in the QGP at temperatures under consideration.

## 5. Expectations for Strange Hadron Production at RHIC

We now combine all recent advances in theoretical models of strangeness production and data interpretation at SPS energies with the objective of making reliable predictions for the RHIC energy range.<sup>83</sup> First we address the question how much strangeness can be expected at RHIC. The numerical study of Eq. (36) becomes possible as soon as we define the temporal evolution of the temperature for RHIC conditions. We expect that a global cylindrical expansion should describe the dynamics: aside of the longitudinal flow, we allow the cylinder surface to expand given the internal thermal pressure. SPS experience suggests that the transverse matter flow will not exceed the sound velocity of relativistic matter  $v_\perp \simeq c/\sqrt{3}$ . We recall that for a pure longitudinal expansion local entropy density scales according to  $S \propto T^3 \propto 1/\tau$ .<sup>88</sup> It is likely that the transverse flow of matter will accelerate the drop in entropy density. We thus consider the following temporal evolution function of the temperature:

$$T(\tau) = T_0 \left[ \frac{1}{(1 + \tau \ 2c/d)(1 + \tau \ v_\perp/R_\perp)^2} \right]^{1/3}. \quad (38)$$

We take the thickness of the initial collision region at  $T_0 = 0.5\text{ GeV}$  to be  $d(T_0 = 0.5)/2 = 0.75\text{ fm}$ , and the transverse dimension in nearly central Au–Au collisions to be  $R_\perp = 4.5\text{ fm}$ . The time at which thermal initial conditions are reached is assumed to be  $\tau_0 = 1\text{ fm}/c$ . When we vary  $T_0$ , the temperature at which the gluon equilibrium is reached, we also scale the longitudinal dimension according to:

$$d(T_0) = (0.5\text{ GeV}/T_0)^3 1.5\text{ fm}. \quad (39)$$

This assures that when comparing the different evolutions of  $\gamma_s$  we are looking at

an initial system that has the same entropy content by adjusting its initial volume  $V_0$ . The reason we vary the initial temperature  $T_0$  down to 300 MeV, maintaining the initial entropy content is to understand how the assumption about the chemical equilibrium of gluons, reached by definition at  $T_0$ , impacts strangeness evolution. In fact when considering decreasing  $T_0$  (and thus increasing  $V_0$ ), the thermal production is turned on at a later time in the history of the collision.

The numerical integration of Eq. (36) is started at  $\tau_0$ , and a range of initial temperatures  $300 \leq T_0 \leq 600$ , varying in steps of 50 MeV. The high limit of the temperature we explore exceeds somewhat the ‘hot glue scenario’,<sup>84</sup> while the lower limit of  $T_0$  corresponds to the more conservative estimates of possible initial conditions.<sup>88</sup> Since the initial  $p$ - $p$  collisions also produce strangeness, we take as an estimate of initial abundance a common initial value  $\gamma_s(T_0) = 0.15$ . The time evolution in the plasma phase is followed up to the break-up of QGP. This condition we establish in view of results of the analysis for SPS presented in section 3. We recall that SPS-analysis showed that the system dependent baryon and antibaryon  $m_\perp$ -slopes of particle spectra are result of differences in collective flow in the deconfined QGP source at freeze-out. In consequence there is universality of physical properties of hadron chemical freeze-out between different SPS systems. This value is nearly applicable to RHIC conditions, as can be seen extrapolating the phase boundary curve to the small baryochemical potentials. The QGP break-up temperature  $T_f^{\text{SPS}} \simeq 143 \pm 5$  MeV will see just a minor upward change, and we adopt here the value  $T_f^{\text{RHIC}} \simeq 150 \pm 5$  MeV.

With the freeze-out condition fixed, one would think that the major remaining uncertainty comes from the initial gluon equilibration temperature  $T_0$ , and we now study how different values of  $T_0$  influence the final state phase space occupancy. We integrate numerically Eq. (36) and present  $\gamma_s$  as function of both time  $t$  in Fig. 5a, and temperature  $T$  in Fig. 5b, up to the expected QGP breakup at  $T_f^{\text{RHIC}} \simeq 150 \pm 5$  MeV. We see that:

- widely different initial conditions (with similar initial entropy content) lead to rather similar chemical conditions at chemical freeze-out of strangeness,
- despite a series of conservative assumptions, we find, not only, that strangeness equilibrates, but indeed that the dilution effect allows an overpopulation of the strange quark phase space. For a wide range of initial conditions, we obtain a narrow band  $1.15 > \gamma_s(T_f) > 1$ . We will in the following, taking into account some contribution from hadronization of gluons in strange/antistrange quarks, adopt what the value  $\gamma_s(T_f) = 1.25$ .

We now consider how this relatively large value of  $\gamma_s$ , characteristic for the underlying QGP formation and evolution of strangeness, impacts the strange baryon and anti-baryon observable emerging in hadronization. Remembering that major changes compared to SPS should occur in rapidity spectra of mesons, baryons and antibaryons, we will apply the same hadronization model that worked in the analysis of the SPS data. This hypothesis can be falsified easily, since based and compared to the Pb–Pb 158A GeV results it implies:

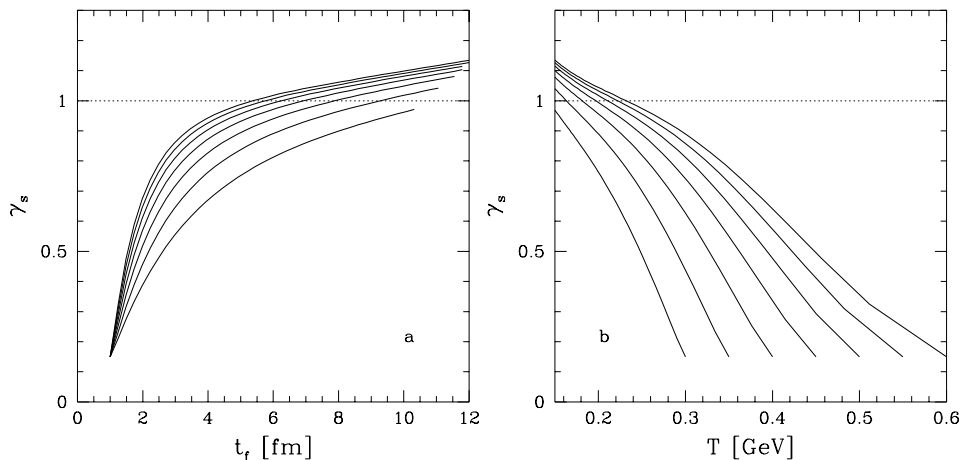


Fig. 5. Evolution of QGP-phase strangeness phase space occupancy  $\gamma_s$ . **a)** as function of time and, **b)** as function of temperature for  $m_s(1 \text{ GeV}) = 200 \text{ MeV}$ , see text for details.

a) shape identity of all RHIC  $m_\perp$  and  $y$  spectra of antibaryons  $\bar{p}$ ,  $\bar{\Lambda}$ ,  $\bar{\Xi}$ , since there is no difference in their production mechanism, and the form of the spectra is determined in a similar way to SPS energy range by the local temperature and flow velocity vector;

b) the  $m_\perp$ -inverse-slopes of these antibaryons should be very similar to the result obtained at CERN for Pb–Pb 158A GeV, since the expected 3% increase in the freeze-out temperature is accompanied by a comparable increase in collective transverse flow.

The abundances of particles produced from QGP within the sudden freeze-out model are controlled by several parameters we addressed earlier: the light quark fugacity  $1 < \lambda_q < 1.1$ , value is limited by the expected small ratio between baryons and mesons (baryon-poor plasma) when the energy per baryon is above 100 GeV, strangeness fugacity  $\lambda_s \simeq 1$  which value for locally neutral plasma assures that  $\langle s - \bar{s} \rangle = 0$ ; the light quark phase space occupancy  $\gamma_q \simeq 1.5$ , overabundance value due to gluon fragmentation. Given these narrow ranges of chemical parameters and the freeze-out temperature  $T_f = 150 \text{ MeV}$ , we compute the expected particle production at break-up. In general, we cannot expect that the absolute numbers of particles we find are correct, as we have not modeled the important effect of flow in the laboratory frame of reference. However, ratios of hadrons subject to similar flow effects (compatible hadrons) can be independent of the detailed final state dynamics, as the results seen at SPS suggest, and we will look at such ratios more closely.

Taking  $\gamma_q = 1.5^{+0.10}_{-0.25}$ , we choose the value of  $\lambda_q$ , see the header of table 7, for which the energy per baryon ( $E/B$ ) is similar to the collision condition (100 GeV), which leads to the range  $\lambda_q = 1.03 \pm 0.005$ . We evaluate for these examples aside of  $E/B$ , the strangeness per baryon  $s/B$  and entropy per baryon  $S/B$  as shown in the

Table 7. For  $\gamma_s = 1.25$ ,  $\lambda_s = 1$  and  $\gamma_q, \lambda_q$  as shown: Top portion: strangeness per baryon  $s/B$ , energy per baryon  $E/B$ [GeV] and entropy per baryon  $S/B$ . Bottom portion: sample of hadron ratios expected at RHIC.

$\gamma_q$	1.25	1.5	1.5	1.5	1.60
$\lambda_q$	1.03	1.025	1.03	1.035	1.03
$E/B$ [GeV]	117	133	111	95	110
$s/B$	18	16	13	12	12
$S/B$	630	698	583	501	571
$p/\bar{p}$	1.19	1.15	1.19	1.22	1.19
$\Lambda/p$	1.74	1.47	1.47	1.45	1.35
$\bar{\Lambda}/\bar{p}$	1.85	1.54	1.55	1.55	1.44
$\bar{\Lambda}/\Lambda$	0.89	0.91	0.89	0.87	0.89
$\Xi^-/\Lambda$	0.19	0.16	0.16	0.16	0.15
$\bar{\Xi}^-/\bar{\Lambda}$	0.20	0.17	0.17	0.17	0.16
$\bar{\Xi}/\Xi$	0.94	0.95	0.94	0.93	0.94
$\Omega/\Xi^-$	0.147	0.123	0.122	0.122	0.115
$\bar{\Omega}/\bar{\Xi}^-$	0.156	0.130	0.130	0.131	0.122
$\bar{\Omega}/\Omega$	1	1.	1.	1.	1.
$\frac{\Omega+\bar{\Omega}}{\Xi^-+\bar{\Xi}^-}$	0.15	0.13	0.13	0.13	0.12
$\frac{\Xi^-+\bar{\Xi}^-}{\Lambda+\bar{\Lambda}}$	0.19	0.16	0.16	0.16	0.15
$K^+/K^-$	1.05	1.04	1.05	1.06	1.05

top section of the table 7. We do not enforce  $\langle s - \bar{s} \rangle = 0$  exactly, but since baryon asymmetry is small, strangeness is balanced to better than 2% in the parameter range considered. In the bottom portion of table 7, we present the compatible particle abundance ratios, computed according to the procedure developed in section 2. We have given, aside of the baryon and antibaryon relative yields, also the relative kaon yield, which is also well determined within this approach.

The meaning of these results can be better appreciated when we assume in an example the central rapidity density of direct protons is  $dp/dy|_{\text{cent.}} = 25$ . In table 8, we present the resulting (anti)baryon abundances. The net baryon density  $db/dy \simeq 16 \pm 3$ , there is baryon number transparency. We see that (anti)hyperons are indeed more abundant than non-strange (anti)baryons. Taking into account the disintegration of strange baryons, we are finding a much greater number of observed protons  $dp/dy|_{\text{cent.}}^{\text{obs.}} \simeq 65 \pm 5$  in the central rapidity region. It is important when quoting results from table 8 to recall that:

1) we have chosen arbitrarily the overall normalization in table 8, only particle ratios were computed, and

2) the rapidity baryon density relation to rapidity proton density is a consequence of the assumed value of  $\lambda_q$ , which we chose to get  $E/B \simeq 100$  GeV per participant.

The most interesting result seen in table 8, the hyperon-dominance of the baryon yields at RHIC, does not depend on detailed model hypothesis. We have explored another set of parameters in our first and preliminary report on this matter,<sup>89</sup> finding this result. Another interesting property of the hadronizing hot RHIC matter,



Table 8.  $dN/dy|_{\text{cent.}}$  assuming in this example  $dp/dy|_{\text{cent.}} = 25$ .

$\gamma_q$	$\lambda_q$	$b$	$p$	$\bar{p}$	$\Lambda+\Sigma^0$	$\bar{\Lambda}+\bar{\Sigma}^0$	$\Sigma^\pm$	$\bar{\Sigma}^\mp$	$\Xi^0$	$\bar{\Xi}^0$	$\Omega=\bar{\Omega}$
1.25	1.03	17	25*	21	44	39	31	27	17	16	1.2
1.5	1.025	13	25*	22	36	33	26	23	13	11	0.7
1.5	1.03	16	25*	21	37	33	26	23	12	11	0.7
1.5	1.035	18	25*	21	36	32	26	22	11	10	0.7
1.60	1.03	15	25*	21	34	30	24	21	10	9.6	0.6

as seen in table 7, is that strangeness yield per participant is expected to be 13–23 times greater than seen at present at SPS energies, where we have 0.75 strange quark pairs per baryon. As seen in table 8, the baryon rapidity density is in this examples similar to the proton rapidity density.

## 6. Summary and Conclusions

We believe that this study of SPS strangeness results decisively shows interesting new physics. We see considerable convergence of the results around properties of suddenly hadronizing QGP.<sup>55</sup> The key results we obtained in the Fermi-2000 model data analysis are:

- 1) the same hadronization temperature  $T=142\text{--}144\text{MeV}$  for very different collision systems with different hadron spectra;
- 2) QGP expected results for the source phase space properties:  $\tilde{\lambda}_s = 1$  for both S- and Pb-collisions, implying  $\lambda_s^{\text{Pb}} \simeq 1.1$ ;
- 3)  $\gamma_s^{\text{Pb}} > 1$ , indicating that a high strangeness yield was reached before freeze-out;
- 4)  $\gamma_q > 1$  as would be expected from a high entropy phase and the associated value  $S/B \simeq 43 \pm 3$ ;
- 5) the yield of strangeness per baryon  $\bar{s}/B \simeq 0.7$  just as predicted by gluon fusion in thermal QGP, a point we studied in detail in section 3.3;
- 6) the transverse expansion velocity for Pb–Pb:  $v_c^{\text{Pb}} \leq 1/\sqrt{3}$ , just below the sound velocity of quark matter.

The universality of the physical properties at chemical freeze-out for S- and Pb-induced reactions points to a common nature of the primordial source of hadronic particles. The difference in spectra between the two collision systems considered arises, in this analysis, due to the difference in the degree of chemical equilibration of light and strange quarks, expected for systems of differing size and lifespan, and a difference in the collective surface explosion velocity,  $v_c^{\text{S}} \simeq 0.5 < v_c^{\text{Pb}} \simeq 1/\sqrt{3}$ , which for larger system is higher, having more time to develop. Considering how small the experimental WA97 spectral slope errors shown in table 3 are presently, there is now overwhelming evidence that the production mechanism of both  $\Lambda$  and  $\bar{\Lambda}$  is the same, which observation is very probably also true for both  $\Xi$  and  $\bar{\Xi}$ . This symmetry between matter–antimatter production is an important cornerstone of the claim that the strange antibaryon data can only be interpreted in terms of direct

emission from a deconfined and thus matter-antimatter symmetric quark matter.

We note that the QGP break-up temperature we find,  $T_f = 143 \text{ MeV}$ , corresponds to an energy density  $\varepsilon = \mathcal{O}(0.5) \text{ GeV/fm}^3$ .<sup>90</sup> Among other interesting results which also verify the consistency of the experimental data understanding within the Fermi-2000 model, we recall:

- the exact balancing of strangeness  $\langle \bar{s} - s \rangle = 0$  also in the final hadronic particles in the symmetric Pb–Pb case;
- the increase of the baryochemical potential  $\mu_B^{\text{Pb}} = 203 \pm 5 > \mu_B^{\text{S}} = 178 \pm 5 \text{ MeV}$  as the collision system grows;
- the energy per baryon near to the value expected if energy and baryon number deposition in the fireball are similar;
- hadronization into pions at  $\gamma_q \rightarrow \gamma_q^c = e^{m_\pi/2T_f} \simeq 1.6$  seen in Pb–Pb reactions, which is an effective way to convert excess of entropy in the plasma into hadrons, without need for reheating, or a mixed phase; the finding of the maximum allowable  $\gamma_q$  is intrinsically consistent with the notion of an explosively disintegrating QGP phase.

A reassuring feature of the Pb–Pb analysis related to chemical equilibration has been described in subsection **2.3**: we find a pion yield which maximizes the entropy density of hadronic particles produced.<sup>56</sup> This detailed technical result explains how sudden hadronization can occur: in general the deconfined state with broken color bonds and thus the high entropy density has to find an exit into the hadronic world, maintaining or increasing the total entropy and preferentially also the local entropy contained within a small, comoving volume cell. Our analysis of experimental results suggests that this is accomplished by generating an over-saturated pion phase space, in which the entropy density rises to values as high as are believed to occur in QGP at hadronization. Chemical equilibrium hadronization requires the formation of a mixed plasma-hadron gas phase and is generally believed to require a relatively long time, followed by kinetic reequilibration. In our opinion such a hadronization model is now inconsistent with the experimental strange baryon and antibaryon data on yields and spectra. The reader should note that such technical differences between different groups about the dynamics of the evolution of the hadron fireball *after* the deconfined phase has hadronized, do not impact the primary agreement about the deconfined nature of the high density source of hadronic particles.

We believe that omission to consider chemical non-equilibrium in the study of freeze-out conditions employing the analysis of spectral shape (flow) and also pion correlation (HBT) effect is the source of the difference of results here presented with some other recent work.<sup>91,92</sup> To understand the source of this difference it is important to realize that there is a considerable influence on the shape of pion spectra by the light quark chemical non-equilibrium which the data analysis presented includes: the cocktail of resonance decays contributing to pion spectra is altered, and moreover, there is spectral deformation at low  $m_\perp$  due to pion correlation effects caused by the overpopulated phase space.<sup>56</sup> We note that results presented also differ somewhat from the WA98 experiment analysis addressing solely  $\pi^0$  spectra, and

which again assumes pion chemical equilibrium.<sup>92</sup> In consequence, the  $\pi^0$ -freeze-out conditions as seen in Ref. <sup>92</sup>, Table 1 are different from those determined here. On the other hand, another recent hadron spectral shape analysis,<sup>93</sup> which did not introduce low  $m_{\perp}$  pion spectra into consideration obtains a chemical freeze-out conditions nearly identical to those we discussed. While the precise understanding of hadronization condition is required for a measurement of physical properties of QGP including the latent heat, the differences discussed are of little if any consequence concerning the fundamental issue, the question if deconfinement is achieved.

The sudden hadronization of entropy rich QGP leads to value  $\gamma_q \rightarrow \gamma_q^c$ , in order to connect the entropy rich deconfined and the confined phases more efficiently. The dominant pion contribution to the entropy density (and pressure) is nearly twice as high at  $\gamma_q \simeq \gamma_q^c$  than at  $\gamma_q = 1$ . Without this phenomenon one has to introduce a mechanism that allows the parameter  $VT^3$  to grow, thus expanding either the volume  $V$  due to formation of the mixed phase or invoking a rise of  $T$  in the reheating. The range of values for  $\gamma_q$  is bounded from above by the Bose distribution singularity  $\gamma_q \rightarrow \gamma_q^c$ , but a pion condensate is not formed since it ‘consumes’ energy without consuming entropy of the primordial high entropy QGP phase. An interesting feature of such a mechanism of phase transition which side-steps the need to form a mixed phase or reheating is that the chemical non-equilibrium reduces and potentially eliminates any discontinuity in the phase transition. This being the case, experimental searches will not find the critical fluctuations expected for a discontinuous phase change, even if theory implies a 1st order phase transition for the statistical equilibrium system. This is in agreement with the failure of NA49 experiment to find precritical fluctuations in event-by-event analysis.<sup>94</sup>

The only not fully quantitatively described particle yields are  $\Omega$  and  $\bar{\Omega}$ : for the parameters we find, the Fermi-2000 model applied to Pb–Pb reactions underpredicts this smallest of all hadronic abundances by about factor 2. This means that we expect, within the sudden hadronization of QGP with uncorrelated strange quarks in the deconfined phase, only an enhancement of  $\Omega$  and  $\bar{\Omega}$  yields by a factor 8-10 as compared to what is expected from extrapolation of p–A reactions. Since the experiment reports an enhancement by factor 15–20, we need to think again. This ‘failure’ of Fermi-2000 model is in fact confirming the early expectation that  $\Omega$  and  $\bar{\Omega}$  yields are the best signature of deconfinement,<sup>11</sup> we just must in future address the question what exactly this tells us about QGP structure. We have argued nearly 20 years ago that strangeness pairing in the color anti-triplet channel  $(ss)_{\bar{3}}$  in the QGP source would enhance  $\Omega$  and  $\bar{\Omega}$  yields,<sup>11</sup> a point that is of some topical interest today in context of color superconductivity studies.<sup>79</sup>

Despite this unexpected additional enhancement, we firmly conclude in view of all diverse evidence that (multi)strange hadronic particles seen at CERN-SPS are emerging from a deconfined QGP phase of hadronic matter and do not undergo a re-equilibration after they have been produced. This finding has encouraged us to consider within the same computational scheme the production of strange hadrons at RHIC conditions. First, we have shown that one can expect strangeness chem-

ical equilibration in nuclear collisions at RHIC if the deconfined QGP is formed. There will, as at SPS, be overpopulation effect associated with the early strangeness abundance freeze-out before hadronization. Most importantly for signatures of new physics at RHIC, we found that strange (anti)baryon abundances will be greater than the yields of non-strange baryons (protons, neutrons). Consequently, the rapidity distributions of (anti)protons are arising from decays of (anti)hyperons.

We are not aware that microscopic model studies reported in the literature about RHIC conditions which have noted this remarkable hyperon dominance result, see, *e.g.*, Ref. <sup>95</sup>. The reader could wonder why is this unusual phenomenon not happening at SPS energies described in section 3? At SPS there is still an appreciable relative baryon abundance among all hadrons (about 15%) and the strangeness yield is at SPS energies only at a level similar to the baryon yield. Thus while abundant (anti)hyperon formation begins to set in, there are still many non-strange (anti)baryons produced. With increasing per baryon energy the yield of strange quark pairs per baryon rises, and at the same time the relative abundance of baryons among all hadrons diminishes. As result, at RHIC energies, we have predicted that hyperons and/or antihyperons are the dominant population fraction among all baryons and/or antibaryons. We thus believe that the preponderance of hyperons as the dominant (anti)baryon population at RHIC energies can be uniquely correlated with the formation and sudden hadronization of deconfined QGP phase.

In a nutshell: we find that strangeness and (anti)baryon QGP signatures are conclusively proving formation of deconfined quark matter phase at SPS energies, and that these signatures of new physics are much more distinct at higher RHIC energies.

*Acknowledgment:* We thank the editor of *Int. J. Mod. Phys. E*, Ernest Henley, and Keith Dienes for valuable comments and suggestions.

## References

1. H. Fritzsch, M. Gell-Mann and H. Leutwyler, *Phys. Lett. B* **47**, 365 (1973).
2. H.D. Politzer, *Phys. Rep.* **14**, 129 (1974).
3. For a bibliographic review of the subject and its roots, see: J. Harris and B. Müller, *Ann. Rev. Nucl. Part. Sci.* **46**, pp.71-107 (1996).
4. See the web page:  
<http://www.cern.ch/CERN/Announcements/2000/NewStateMatter/>  
 Text of the scientific consensus view of the spokesmen of CERN experiments is also available as E-print: nucl-th/0002042, "Evidence for a New State of Matter: An Assessment of the Results from the CERN Lead Beam Program me", compilation by U. Heinz, and Maurice Jacob
5. J. Rafelski and M. Danos, *Perspectives in High Energy Nuclear Collisions*, NBS-IR 83-2725 Monograph, U.S. Department of Commerce, National Bureau of Standards, June 1983;  
 Updated version appeared in *Nuclear Matter under Extreme Conditions*, D. Heiss, Ed., Springer Lecture Notes in Physics **231**, pp.362-455 (1985).

6. F.R. Brown *et al.*, *Phys. Rev. Lett.* **65**, 2491 (1990).
7. T. Blum, L. Kärkkäinen, D. Toussaint, S. Gottlieb, *Phys. Rev. D* **51**, 5153 (1995).
8. C. DeTar, “Quark Gluon Plasma in Numerical Simulations of Lattice QCD”, in *Quark Gluon Plasma 2*, p.1, R.C. Hwa (Eds.), World Sci., (Singapore 1995).
9. M. Stephanov, K. Rajagopal and E. Shuryak, *Phys. Rev. Lett* **81**, 4816 (1998).
10. K. Rajagopal, *Nucl. Phys. A* **661**, 150 (1999).
11. J. Rafelski, “Extreme States of Nuclear Matter”, pp.282–324, in *Future Relativistic Heavy Ion Experiments*, R. Bock and R. Stock, Eds., GSI Report 1981-6;  
J. Rafelski, in *New Flavor and Hadron Spectroscopy*, J. Tran Thanh Van, Ed., p. 619, Editions Frontières (Paris 1981);  
J. Rafelski, *Nucl. Physics A* **374**, 489c (1982);  
J. Rafelski, *Phys. Rep.* **88**, 331 (1982).
12. J. Rafelski and B. Müller, *Phys. Rev. Lett* **48**, 1066 (1982); **56**, 2334E (1986);  
P. Koch, B. Müller and J. Rafelski, *Z. Phys. A* **324**, 453 (1986).
13. P. Koch, B. Müller and J. Rafelski, *Phys. Rep.* **142**, 167 (1986).
14. “Strangeness and Quark Gluon Plasma: Aspects of Theory and Experiment” H.C. Eggers and J. Rafelski, *Int. J. Mod. Phys. A* **6**, 1067, (1991).
15. J. Rafelski, *Phys. Lett. B* **262**, 333 (1991); *Nucl. Phys. A* **544**, 279c (1992).
16. J. Rafelski, J. Letessier and A. Tounsi, *Acta Phys. Pol. B* **27**, 1035 (1996).
17. T. Matsui, B. Svetitsky and L.D. McLerran, *Phys. Rev. D* **34**, 783 and 2047 (1986).
18. N. Bilic, J. Cleymans, I. Dadić and D. Hislop, *Phys. Rev. C* **52**, 401 (1995).
19. P. Koch and J. Rafelski, *Nucl. Phys. A* **444**, 678 (1985).
20. J. Letessier, A. Tounsi and J. Rafelski, *Phys. Lett. B* **390**, 363 (1997).
21. F. Antinori *et al.*, the WA97 Collaboration, “Transverse mass spectra of strange and multi-strange particles in Pb–Pb collisions at 158A GeV/c”, CERN preprint CERN-EP-2000-001
22. F. Antinori, *et al.*, WA97 collaboration, *Nucl. Phys. A* **661**, 130c (1999)
23. F. Antinori, *et al.*, WA97 collaboration, *Eur. Phys. J. C* **11**, 79 (1999).
24. E. Andersen *et al.*, WA97 collaboration, *Phys. Lett. B* **433**, 209 (1998).
25. R. Lietava, *et al.*, WA97 collaboration, *J. Phys. B* **25**, 181 (1999).
26. H. Appelshäuser *et al.*, NA49, *Phys. Lett. B* **444**, 523 (1998).
27. F. Antinori *et al.*, WA85 collaboration, *Phys. Lett. B* **447**, 178 (1999).
28. Th. Alber *et al.*, NA35 collaboration, *Z. Phys. C* **64**, 195 (1994).
29. D. Evans *et al.*, WA85 and WA94 collaboration, *J. Phys. G Nucl. Part. Phys.*, **25**, 209 (1999).
30. H. Boggild *et al.*, NA44 Collaboration, *Phys. Rev. C* **59**, 328 (1999).
31. E. Andersen *et al.*, WA97 collaboration, *Phys. Lett. B* **449**, 401 (1999).
32. F. Siklér, *et al.*, NA49 collaboration, *Nucl. Phys. A* **661**, 45c (1999).
33. I. Bearden, *et al.*, NA44 collaboration, *Phys. Lett. B* **471**, 6 (1999).
34. S. Kabana *et al.*, NA52 collaboration, *Nucl. Phys. A* **661**, 370c (1999);  
S. Kabana *et al.*, NA52 collaboration, *J. Phys. G Nucl. Part. Phys.* **25**, 217 (1999).
35. T. Alber *et al.*, NA49 Collaboration, *Phys. Rev. Lett.* **75**, 3814 (1995).
36. H. Appelshäuser *et al.*, NA49, *Phys. Rev. Lett.* **82**, 2471 (1999).
37. J. Rafelski and J. Letessier, *Acta Phys. Pol. B* **30**, 3559 (1999), presented in June 1999 at the 29th Kraków School of Theoretical Physics, Zakopane, Poland. We thank editors of Acta Physica Polonica for permission to reprint partially sections 2–6 of this manuscript in this review.
38. E. Fermi, *Progr. Theor. Phys.* **5** 570 (1950); *Phys. Rev.* **81**, 115 (1950); *Phys. Rev.* **92**, 452 (1953).
39. R. Hagedorn, *Suppl. Nuovo Cimento* **2**, 147 (1965); Cargèse lectures in Physics, Vol. **6**, Gordon and Breach (New York 1977) and references therein; see also contributions in:

- J. Letessier, H. Gutbrod and J. Rafelski, *Hot Hadronic Matter*, Plenum Press NATO-ASI series B346, New York (1995);  
H. Grote, R. Hagedorn and J. Ranft, *Particle Spectra*, CERN black report (1970).
40. J. Letessier, *et al.*, *Phys. Rev. Lett.* **70**, 3530 (1993).
  41. J. Letessier, *et al.*, *Phys. Rev. D* **51**, 3408 (1995).
  42. K.S. Lee, U. Heinz and E. Schnedermann, *Z. Phys. C* **48**, 525 (1990);
  43. E. Schnedermann, *et al.*, pp.175–206 in *Particle Production in Highly Excited Matter*, NATO-ASI Series B303, H.H. Gutbrod and J. Rafelski, Eds., (Plenum, New York, 1993).
  44. J. Letessier and J. Rafelski, *Phys. Rev. C* **59**, 947 (1999).
  45. J. Letessier and J. Rafelski, *J. Phys. G, Nucl. Part. Phys.* **25**, 295 (1999).
  46. P. Braun-Munzinger, I. Heppe, and J. Stachel, *Phys.Lett. B* **465**, 15 (1999).
  47. J. Cleymans and K. Redlich, *Phys. Rev. C* **60**, 054908 (1999), and references therein.
  48. J. Cleymans and H. Satz, *Z. Physik C* **57**, 135 (1993).
  49. A. Bialas, *Phys.Lett. B* **466**, 301 (1999).
  50. *Hard Processes in Hadronic Interactions*, H. Satz and X.-N. Wang, Eds., special issue of *Int. J. Mod. Phys. A* **10p** 2881 (1995).
  51. S. Bass *et al.*, “Last Call for RHIC Predictions” e-Print: nucl-th/9907090, May 1999; to appear in: Proceedings of 14th International Conference on Ultrarelativistic Nucleus-Nucleus Collisions (QM 99), Torino, Italy, 10-15 May 1999.
  52. J. Sollfrank, *J. Phys. G, Nucl. Part. Phys.* **23**, 1903 (1997).
  53. F. Becattini, M. Gazdzicki and J. Sollfrank, *Eur. Phys. J. C* **5**, 143 (1998).
  54. J. Letessier and J. Rafelski, *Acta Phys. Pol. B* **30**, 153 (1999).
  55. J. Rafelski and J. Letessier, “Hadrons from Pb-Pb Collisions at 158A GeV” e-Print Archive: nucl-th/9903018.
  56. J. Letessier, J. Rafelski and A. Tounsi, “Low- $m_{\perp}$   $\pi^{+}$ - $\pi^{-}$  Asymmetry Enhancement from Hadronization of QGP”, *Phys. Lett. B* in press (2000), nucl-th/9911043.
  57. K.G. Librecht, and S.E. Koonin, *Phys. Rev. Lett.* **43**, 1581 (1979);  
S. Pratt, *Phys. Rev. D* **33**, 72 (1986);  
S. Pratt, T. Csorgo, and J. Zimanyi, *Phys. Rev. C* **42**, 2646 (1990);  
G. Baym, and P. Braun-Münzinger, *Nucl. Phys A* **610**, 286c (1996)
  58. B. Muller and J. Rafelski, *Phys. Rev. Lett.* **34**, 349 (1975).
  59. J. Letessier, A. Tounsi and J. Rafelski, *Phys. Rev. C* **50**, 406 (1994);  
J. Rafelski, J. Letessier and A. Tounsi, *Acta Phys. Pol. A* **85**, 699 (1994).
  60. J. Sollfrank, *et al. Z. Physik. C* **61**, 659 (1994).
  61. G.J. Odyniec, *Nucl. Phys. A* **638**, 135 (1998).
  62. F. Pühlhofer, *et al.*, NA49 collaboration, *Nucl. Phys. A* **638**, 431 (1998).
  63. C. Bormann, *et al.*, NA49 collaboration, *J. Phys. G, Nucl. Part. Phys.* **23**, 1817 (1997).
  64. I. Králik, *et al.*, WA97 collaboration, *Nucl. Phys. A* **638**, 115 (1998).
  65. S. Abatzis *et al.*, WA85 Collaboration, *APH N.S., Heavy Ion Physics* **4**, 79 (1996).
  66. G.J. Odyniec, for the NA49 Collaboration, *J. Phys. G, Nucl. Part. Phys.* **23**, 1827 (1997).
  67. D. Röhrig, for the NA49 Collaboration, “Recent results from NA49 experiment on Pb–Pb collisions at 158 A GeV”, see Fig.4, in proc.of EPS-HEP Conference, Jerusalem, Aug. 19-26, 1997. D. Lellouch *et al.*, Eds., Springer (Berlin, 1999), pp. 613-618.
  68. P.G. Jones, for the NA49 Collaboration, *Nucl. Phys. A* **610**, 188c (1996).
  69. H. van Hecke, H. Sorge and N. Xu, *Phys. Rev. Lett.* **81**, 5764 (1998).
  70. S.A. Bass *et al. Phys. Rev. C* **60**, 021902 (1999).
  71. J. Cleymans and K. Redlich, *Phys. Rev. Lett.* **81**, 5284 (1998); and Ref. <sup>47</sup>.
  72. J.C. Dunlop and C.A. Ogilvie, *Phys. Rev. C* **61**, 031901(R), (2000).
  73. C. Greiner, P. Koch, and H. Stöcker, *Phys. Rev. Lett.* **58**, 1825 (1987).

74. J. Rafelski, *Phys. Lett. B* **190**, 167 (1987).
75. U. Heinz, K. S. Lee, and M. J. Rhoades Brown, *Mod. Phys. Lett. A* **2**, 153 (1987).
76. C. Greiner, and H. Stöcker, *Phys. Rev. D* **44**, 3517 (1991).
77. J. Letessier, J. Rafelski and A. Tounsi, *Phys. Lett. B* **410**, 315 (1997).
78. A.K. Holme, *et al.*, WA97 collaboration, *J. Phys. G Nucl. Part. Phys.*, **23**, 1851 (1997).
79. M. Alford, K. Rajagopal, and F. Wilczek, *Nucl. Phys. A* **638**, 515c (1998);  
R.D. Pisarski, and D.H. Rischke, *Phys. Rev. D* **60**, 4013 (1999);  
T. Schafer, *Nucl. Phys. A* **661** 621C (1999).
80. T.S. Biró, E. van Doorn, B. Müller, M.H. Thoma and X.-N. Wang, *Phys. Rev. C* **48**, 1275 (1993).
81. S.M.H. Wong, *Phys. Rev. C* **54**, 2588 (1996); and **56**, 1075 (1996), and references therein.
82. D.K. Srivastava, M.G. Mustafa and B. Müller, *Phys. Lett. B* **396**, 45 (1997); *Phys. Rev. C* **56**, 1054 (1997).
83. J. Rafelski and J. Letessier, *Phys. Lett. B* **469**, 12 (1999).
84. E. Shuryak, *Phys. Rev. Lett.* **68**, 3270 (1992).
85. Jan-e Alam, S. Raha and B. Sinha, *Phys. Rev. Lett.* **73**, 1895 (1994);  
P. Roy, Jan-e Alam, S. Sarkar, B. Sinha, and S. Raha, *Nucl. Phys. A* **624**, 687 (1997).
86. S.M.H. Wong *Phys. Rev. C* **56**, 1075 (1997).
87. J. Rafelski, J. Letessier and A. Tounsi, *APH N.S., Heavy Ion Physics*, **4**, 181 (1996);  
J. Letessier, J. Rafelski, and A. Tounsi, *Phys. Lett. B* **389**, 586 (1996).
88. J.D. Bjorken, *Phys. Rev. D* **27**, 140 (1983).
89. <http://www.qm99.to.infn.it/program/qmprogram.html>  
Presentation on Friday, May 24, 1999 at 11:25AM by J. Rafelski; to appear in proceedings of *Quark Matter 1999*, Torino, Italy within a group report “*Last call for RHIC predictions*”. S. Bass *et. al.*, nucl-th/9907090.
90. F. Karsch, and M. Lütgemeier, *Nucl. Phys. B* **550**, 449 (1999).
91. B. Tomásik, U.A. Wiedemann and U. Heinz, “Reconstructing the Freeze-out State in Pb+Pb Collisions at 158A GeV/c”, electronic preprint nucl-th/9907096.
92. M.M. Aggarwal *et al.*, WA98 Collaboration *Phys. Rev. Lett.* **83**, 926 (1999).
93. B.R. Schlei, D. Strottman, J.P. Sullivan, and H.W. van Hecke, *Eur.Phys. J. C* **10**, 483 (1999).
94. H. Appelshauser *et al.*, NA49 Collaboration *Phys. Lett. B* **459**, 679 (1999).
95. A. Dumitru, S.A. Bass, M. Bleicher, H. Stöcker and W. Greiner *Phys. Lett. B* **460**, 411 (1999).